ELSEVIER

Journal of Structural Geology 29 (2007) 355–374

JOURNAL OF STRUCTURAL GEOLOGY

www.elsevier.com/locate/jsg

Brittle-ductile microfabrics in naturally deformed cordierite: Evidence for significant short-term strain-rate variations

Jörn H. Kruhl [a,*,1], Saskia Erdmann [b,1], Steffen H. Büttner [c]

[a] *Tectonics and Material Fabrics Section, Faculty of Civil and Geodetic Engineering, Technische Universität, D-80290 München, Germany*
[b] *Institut für Angewandte Geowissenschaften, Technische Universität, Berlin, Germany*
[c] *Department of Geology, Rhodes University, Grahamstown 6140, South Africa*

Received 16 August 2005; received in revised form 8 September 2006; accepted 12 September 2006
Available online 9 November 2006

Abstract

Brittle and ductile microfabrics in cordierite from a migmatite were studied by universal-stage method and electron probe micro-analysis. The microfabrics record crystal fracturing and ductile deformation of one deformation event at ~570 °C and ~380 MPa, but at variable strain rates. The cordierite microfabrics evolve in four stages. (1) At strain rates of $\geq \sim 10^{-7}$ [s^{-1}] brittle micro shear zones form, producing rotated fine-grained cordierite crystal fragments. (2) At decreasing strain rates (001), (010), and (100) subgrain boundaries develop and fluid circulation leads to partial cordierite breakdown and oriented growth of sillimanite, staurolite, magnetite, and quartz along shear planes. (3) Subsequent to deformation and during continuous infiltration of fluids, the same minerals grow randomly along shear planes and cordierite recrystallizes statically. (4) During continuous annealing and fluid infiltration the recrystallized cordierite grains coarsen and sillimanite, staurolite, magnetite, and quartz form along the grain boundaries. Brittle high-temperature and high-strain-rate microfabrics, followed by ductile high-temperature deformation at lower strain rates and/or by recovery, as recorded in the cordierite studied, may be more common in naturally deformed rocks than typically assumed. This is evidence for and may be used as an analytical tool to detect paleo-seismic events.

Keywords: Cordierite; Brittle deformation; Ductile deformation; Microfabrics; Paleo-seismicity; Strain rate

1. Introduction

Low-temperature cordierite, $(Mg,Fe)_2Al_4Si_5O_{18}(n\cdot H_2O)$ (Gibbs, 1966), is a characteristic phase in many metapelites, peraluminous magmatic rocks, and in aluminous gneisses formed at relatively low pressures (e.g., review by Deer et al., 1993). During deformation and metamorphism, cordierite develops brittle and ductile microfabrics similar to other rock-forming minerals such as quartz, calcite, plagioclase, and K-feldspar: micro-fractures, wavy extinction, micro shear zones, subgrains, recrystallized grains, sutured grain boundaries, and deformation twins (van Roermund and Konert, 1990; Kruhl and Huntemann, 1991; Vernon, 2004, p. 330). The formation of those microfabrics is affected dominantly by temperature and strain rate (Hobbs et al., 1976; Vernon, 2004; Passchier and Trouw, 2005). Therefore, the analysis of cordierite microfabrics may allow constraining the temperature and deformation history of a rock. However, only little information is available on the temperature range of cordierite ductility and on how the various deformation microfabrics develop at different temperatures and deformation conditions. A better understanding of the deformation behaviour of cordierite would proof particularly useful in combination with the possibility of using many well established petrological cordierite geothermometers and geobarometers (e.g., Holdaway and Lee, 1977; Vielzeuf, 1983; Bhattacharya et al., 1988).

In this paper we present new data on (i) the development of micro shear zones at the strain-rate related brittle-ductile transition, (ii) crystallographic orientations of recrystallized

* Corresponding author. Tel./fax: +49 89 2891 3168.
E-mail address: kruhl@tum.de (J.H. Kruhl).
[1] Present address: Department of Earth Sciences, Dalhousie University, Halifax, NS B3H 4J1, Canada.

0191-8141/$ - see front matter © 2006 Elsevier Ltd. All rights reserved.
doi:10.1016/j.jsg.2006.09.002

cordierite grains within micro shear zones and of cordierite grain and subgrain boundaries, and (iii) the rotation of subgrains within large cordierite grains adjacent to micro shear zones. We discuss the brittle to ductile microstructure evolution of the cordierite studied and show how a variation in strain rate played a critical role in the formation of the textures observed.

2. The samples studied: geological framework and microfabrics

The samples studied are low-pressure, leucosome-depleted, cordierite-bearing migmatites from the Sierra de Quilmes, northern Sierras Pampeanas, NW Argentina. These migmatites derive from Neoproterozoic to Early Cambrian pelites and greywackes that experienced up to granulite facies low pressure metamorphism in the Early Ordovician (Büttner et al., 2005 and references therein). The samples come from the garnet-cordierite-sillimanite zone, in which the regional metamorphism reached maximum conditions of 750–800 °C at ~600 MPa (Büttner et al., 2005). Prograde crustal heating under static or low-strain conditions was followed by non-penetrative extensional tectonics commencing at the thermal peak and continuing during retrograde near-isobaric cooling. The retrograde shearing of the migmatites ended at low amphibolite facies *P-T* conditions in the uppermost Ordovician (~440 Ma, Büttner et al., 2005).

The studied migmatite samples 'Cafayate' and 496A comprise cordierite, garnet, biotite, quartz, plagioclase, K-feldspar, sillimanite, and accessories. Zones of coarse-grained cordierite, garnet, biotite, quartz, plagioclase, and K-feldspar (~70 Vol%) showing migmatitic fabrics alternate irregularly with zones of fine-grained to medium-grained quartz, plagioclase, K-feldspar, biotite, sillimanite, and cordierite (~30 Vol%). The texture of the migmatite is predominantly characterized by abundant, ~100–500 μm wide, inter- and intracrystalline micro shear zones, with a spacing of ~1–5 mm. The shear zones are generally defined by grain-size reduction and by strongly aligned, fibrous sillimanite, fine-grained biotite, recrystallized grains of cordierite, quartz, plagioclase, and K-feldspar, and zones of intense polygonization of cordierite (Fig. 1).

All rock-forming minerals show evidence for brittle and/or ductile deformation. The several mm to ~2 cm large cordierite grains, hereafter referred to as 'old cordierite grains', are commonly characterized by deformation twinning, grain-boundary suturing and mainly along micro shear zones by recrystallization and subgrain formation (polygonization) (Fig. 2A–E). In contact to plagioclase cordierite partly exhibits strong ductile deformation whereas plagioclase shows only weak kinking and mechanical twinning or no deformation textures. Hence, cordierite appears to be more deformed than plagioclase. Subhedral several cm large garnet has abundant, partly parallel, micro-fractures (Fig. 1). Biotite is ≤2 mm, typically bent and kinked and, along the micro shear zones, fine-grained and strongly aligned, as a result of

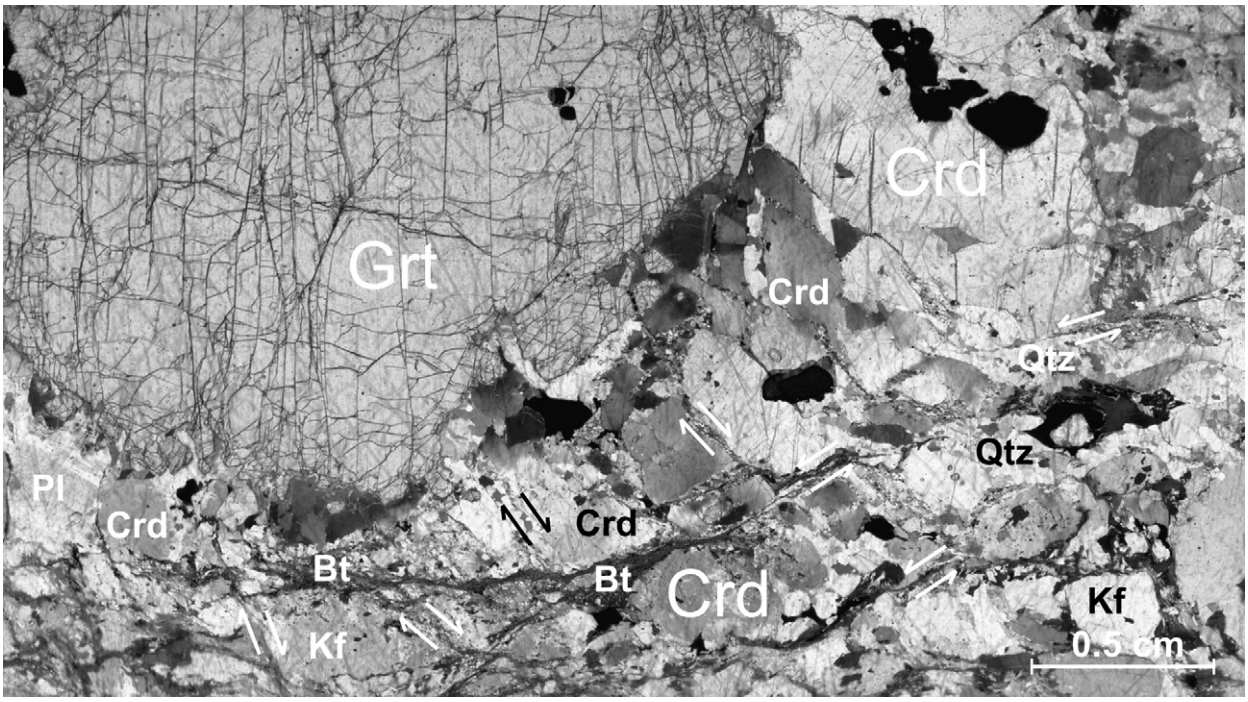

Fig. 1. Photomicrograph of the sample studied (sample 'Cafayate', section A1); strongly oblique polarizers. Coarse-grained cordierite (Crd) and garnet (Grt) dominate the leucosome. Fine- to medium-grained quartz (Qtz), plagioclase (Pl), K-feldspar (Kf), and biotite (Bt) dominate the mesosome. Conjugate, inter- and intracrystalline, sinistral and dextral, micro shear zones (half arrows) are abundant. In the strongly fractured garnet one dominant set of parallel fractures is developed ('vertical' in the photomicrograph), which possibly represents the continuation of the dextral micro shear zones.

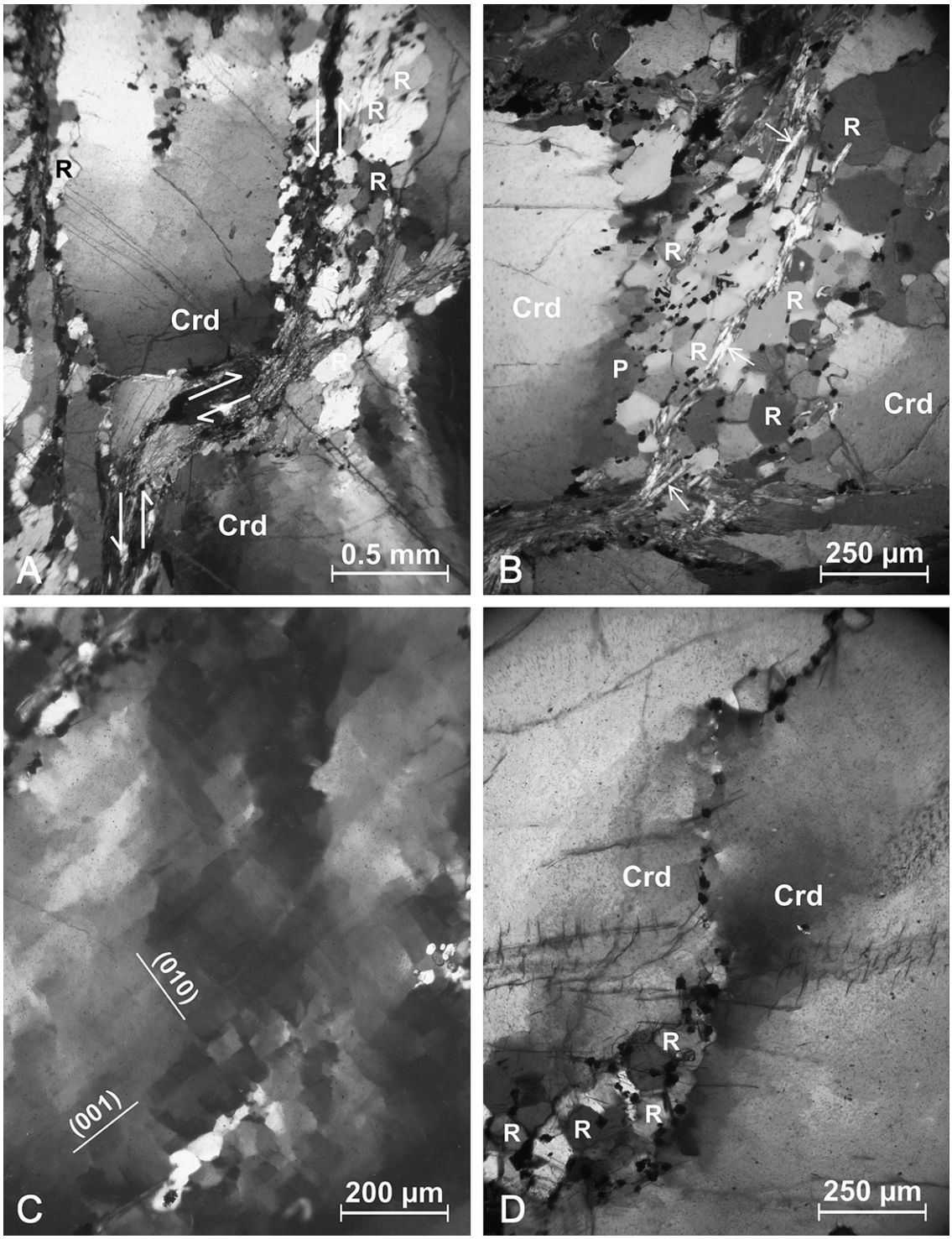

Fig. 2. Photomicrographs (crossed, partly oblique, polarizers) of cordierite deformation fabrics. Sample 'Cafayate', sections A1 and A3. (A) Large old cordierite grain (Crd) transected by sinistral and dextral micro shear zones (half arrows). Sillimanite, biotite, and magnetite are concentrated and partly aligned in the shear-zone centres which are rimmed by recrystallized small cordierite grains (R) oriented with their long axes oblique to the shear zone. (B) Old cordierite (Crd) polygonized and recrystallized along a micro shear zone. The micro shear zone branches into several parallel shear planes outlined by aligned sillimanite needles (arrows), as well as staurolite and magnetite (opaques). One side of the zone of recrystallized cordierite grains (R) is accompanied by a thin stripe of strong polygonization (P) of the old grain, with subgrains of smaller size than the recrystallized grains. On the other side, the old grain is only weakly polygonized. Both contacts are sharp, i.e., with a high misorientation between the crystallized grains and the old grain. (C) Subgrain chessboard pattern in cordierite, composed of subgrain boundaries parallel to (010) and (001). (D) Polygonized old cordierite grain (Crd) transected by a healed fracture which is outlined by small, polygonal, statically recrystallized cordierite grains (R), rare sillimanite needles, as well as staurolite and magnetite (opaques). Along the former fracture, the cordierite is more intensely polygonized than further away. (E) Sutured grain boundary between two old cordierite grains (Crd), which is pinned by magnetite (opaques). The lower part of the photomicrograph is occupied by polygonal recrystallized cordierite grains (R). (F) Statically recrystallized plagioclase (R) along the margin of old, coarse plagioclase grains (Pl). (G) Myrmekite (My) formed at a K-feldspar (Kfs) rim along a micro shear zone with aligned biotite (Bt). The myrmekite is

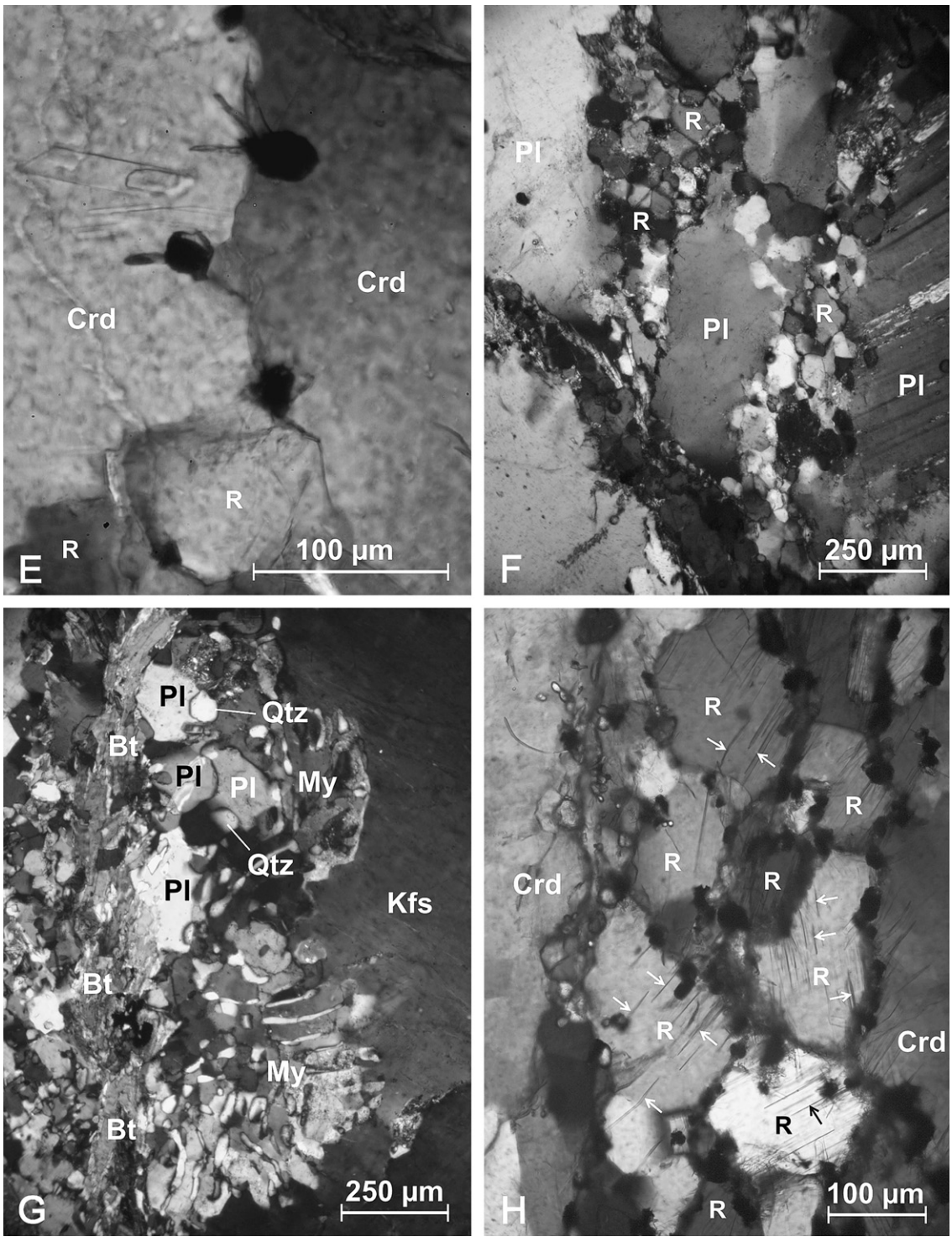

Fig. 2. (*Continued*).

partly recrystallized to a mixture of plagioclase (Pl) and quartz (Qtz) grains. (H) Large cordierite grains (Crd) surrounded by small recrystallized grains (R). The grain boundaries are largely covered by the assemblage sillimanite-staurolite-magnetite (opaques). The parallel sillimanite needles (arrows) in recrystallized as well as host grains are oriented parallel (010), determined by u-stage measurements. (I) Fragments of an old cordierite grain (Crd), partly rotated and partly displaced against each other. The fractures are healed, but outlined by sillimanite, staurolite and magnetite (opaques), cordierite subgrains (S), and, locally, by recrystallized grains (R). Away from the fractures, the old cordierite is only weakly polygonized (broken lines). The space between the cordierite fragments are filled with recrystallized, coarse-grained and strain-free quartz (Qtz). Half arrows indicate sense of shear along fractures. (J) Old cordierite grain (Crd) recrystallized along a sinistral micro shear zone. Concentrations of partly aligned sillimanite needles, staurolite and magnetite (opaques) outline a central shear plane (vertical in the photomicrograph) as well as shear planes branching from the central plane towards the SW (arrows). Sillimanite and opaques rarely cover cordierite grain boundaries perpendicular to, or further away from, the shear planes. The recrystallized grains (R) are partly elongate with their long axes parallel to the shear planes.

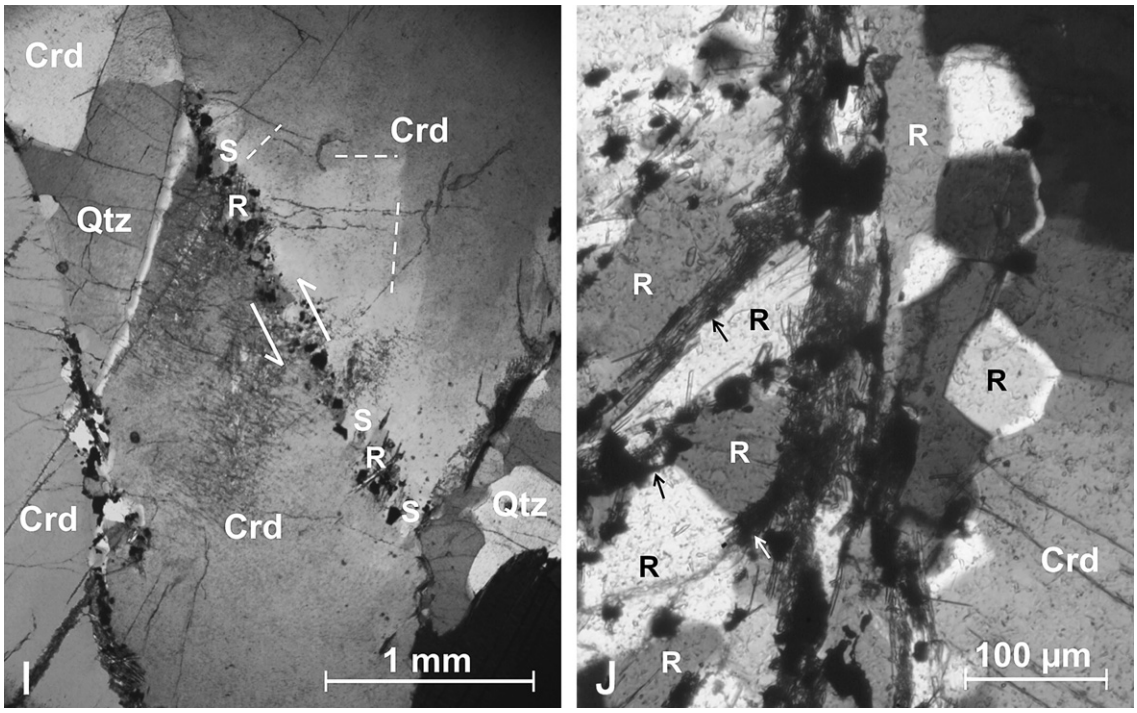

Fig. 2. (*Continued*).

mechanical shearing. Plagioclase is coarse-grained (up to several mm) and subhedral to euhedral. Along micro shear zones in plagioclase strain-free, isometric and polygonal grains—with diameters of ~30–100 µm (average ~60 µm) (Fig. 2F)—indicate static recrystallization. Away from the micro shear zones, plagioclase forms clusters of ~300–800 µm (average ~500 µm) large isometric grains. The up to 1 cm large K-feldspar is characterized by wavy extinction and recrystallized grains of ~50–100 µm along micro shear zones. Coarse-grained myrmekite commonly has formed along K-feldspar margins (Fig. 2G). Quartz between coarse-grained cordierite, K-feldspar and plagioclase is statically recrystallized and has only slightly facetted grain boundaries. The recrystallized quartz grains typically show weak subgrain patterns with prism-parallel subgrain boundaries. Few coarse-grained quartz crystals, away from the micro shear zones, are characterized by weak chessboard patterns. Magnetite forms irregular up to 100 µm large symplectitic grains dominantly along grain boundaries of old and recrystallized cordierite grains (Fig. 2B,D,E,H) or together with biotite and sillimanite within the intercrystalline micro shear zones (Fig. 2A,I,J), but not within zones of recrystallized quartz or feldspar. Sillimanite is fibrous. Together with fine-grained biotite, up to 250 µm long sillimanite needles occur within and typically aligned parallel to the micro shear zones (Fig. 2A,B,J). Up to 100 µm long sillimanite needles occur dominantly along grain boundaries of the old and recrystallized cordierite grains. They are preferentially oriented along (010) planes in old and new crystals (Fig. 2H) but have also random orientation. Together with sillimanite and magnetite, less than 30 µm large euhedral staurolite has formed along the grain boundaries of old and recrystallized cordierite and along intercrystalline micro shear zones.

3. Methods

Given the orthorhombic crystal symmetry of cordierite, the orientation of the cordierite indicatrix is equal to the principal crystallographic directions. Thus, measuring the indicatrix directions of cordierite using a four-axial universal-stage (u-stage—von Federow, 1893; Sarantschina, 1963), the crystallographic orientations of old cordierite grains, subgrains, and recrystallized grains, and the orientation of grain and subgrain boundary facets have been determined. The accuracy of the measurements of the indicatrix axis is approximately ±1° for the azimuth angles and ±2° for the dip (Kuntcheva et al., 2006). However, the u-stage is not feasible for measurements of all grain and subgrain boundaries in a thin section, owing to two reasons: (i) The u-stage tilt is limited to ca. 45° and, therefore, does not allow the rotation of grain or subgrain boundary segments, with a dip of 0–45° in relation to the thin section plane, to a vertical position. Consequently, the orientation of these segments cannot be measured, resulting in an incomplete data set and in the overrepresentation of the measured populations. To overcome this limitation and to assure that all relevant crystallographic orientations of grain and subgrain boundaries are represented in our data set, we have analysed grains of different orientations and have estimated the inhomogeneity of the population density resulting from the non-random grain orientations. (ii) Grain boundaries segmented below the thin-section surface may appear diffuse and, hence, cannot be measured accurately. However, this effect played only a minor role for the sample studied.

Mineral compositions have been determined using electron probe micro-analysis (EPMA) and SEM-EDS. Wavelength-dispersive analysis was used for quantitative analysis of

cordierite and garnet. Energy-dispersive analysis was applied for semi-quantitative analysis of staurolite and qualitative analysis of magnetite as well as fine-grained sillimanite and quartz. Microchemical analyses were obtained using a wavelength dispersive JEOL JXA 733 Superprobe (ZAF correction) at Rhodes University. We used an accelerating potential of 20 kV and a beam current of 15–18 nA. Natural silicate standards have been used for calibration. Peak signals were measured for 10 s for major and 20 s for minor elements. Beam widths were 5 μm for garnet and 10 μm for cordierite. Tests on samples and standards with larger beam sizes have demonstrated that the analytical conditions did not lead to significant devolatilization of light elements. A HITACHI S-4000 Field Emission SEM equipped with an X-ray spectrometer EDS-PGT system with imaging capability of the Technische Universität Berlin has been used for high-resolution imaging and EDS analyses of fine-grained mineral phases along cordierite grain boundaries. To prove the comparability of EPMA and SEM-EDS analytics cordierite has been analysed using both methods yielding nearly identical results. Representative microprobe and EDS analyses are shown in Table 1.

4. Cordierite microfabrics

Old cordierite grains are commonly characterized by the formation of subgrains (polygonization), by deformation twinning, grain-boundary suturing and, along micro shear zones, by static recrystallization (Fig. 2A–E). In contrast to dynamic recrystallization, static recrystallization is interpreted as result of annealing in the ductile field subsequent to deformation in the brittle field, either in consequence of temperature increase or strain-rate decrease to zero at temperatures that are still high enough for grain-boundary migration (Voll, 1969; Vernon, 2004). Specifically subgrains and recrystallized grains and their crystallographic orientations provide information about the brittle-ductile development of the cordierite and, hence, are presented in more detail as follows.

4.1. Subgrains

Subgrains are the dominant microstructure of the old cordierite grains and gradations to recrystallized grains are rare. Where they occur, the size of subgrains and recrystallized grains is similar, typically ~35–60 μm. (Fig. 2A,C,D). The preferred crystallographic orientations of subgrain boundaries indicate specific preferred glide systems.

Crystallographic orientations of subgrain boundaries from four old cordierite grains have been measured (Fig. 3). They are preferentially oriented in three maxima around (001), (010), and (100), and in diffuse and incomplete girdles between (001) and (010), and (010) and (100), respectively (Fig. 3C). Subgrain boundary orientations in the zone {010},

Table 1
Average composition of cordierite, garnet, and staurolite in samples 'Cafayate' and 496A

	'Cafayate' Grain 1		'Cafayate' Grain 2		Old Crd	Recryst. Crd	496A		Grt 'Cafayate'	Staurolite EDX, normalized oxides %	
	Old grain 1	Recryst. Crd	Old grain 2	Recryst. Crd	Near grt	Near grt	Old Crd	Recryst. Crd	Rim comp.	'Cafayate'	496A3
SiO_2	48.09	48.17	48.30	47.61	48.41	48.72	46.89	47.27	37.13	29.80	29.05
TiO_2	0.01	0.03	0.06	0.03	0.05	0.05	0.00	0.00	0.07	0.00	0.00
Al_2O_3	32.70	33.22	33.76	33.86	33.86	34.14	33.55	33.77	20.66	53.21	54.65
MgO	7.82	8.82	8.05	8.95	8.68	9.07	7.56	8.26	3.16	2.40	2.26
CaO	0.03	0.02	0.02	0.02	0.03	0.02	0.00	0.01	0.91	0.00	0.00
MnO	0.38	0.39	0.32	0.30	0.17	0.19	0.42	0.46	4.51	0.30	0.58
FeO	8.06	6.48	7.97	6.39	6.62	5.55	9.02	7.64	32.58	11.48	11.21
Na_2O	0.11	0.10	0.11	0.09	0.17	0.17	0.21	0.24	–	0.00	0.00
K_2O	0.00	0.00	0.00	0.01	0.30	0.61	0.00	0.07	–	0.00	0.00
ZnO	–	–	–	–	–	–	–	–	–	0.82	0.25
Total	97.20	97.25	98.59	97.26	98.29	98.52	97.66	97.72	99.02	98.00	98.00
Si	5.01	4.98	4.96	4.92	4.96	4.96	4.89	4.90	6.03	4.09	3.97
Ti	0.00	0.00	0.00	0.00	0.00	0.00	0.00	0.00	0.01	0.00	0.00
Al	4.01	4.05	4.08	4.12	4.09	4.10	4.13	4.13	3.96	8.60	8.81
Mg	1.21	1.36	1.23	1.38	1.32	1.37	1.18	1.28	0.77	0.49	0.46
Ca	0.00	0.00	0.00	0.00	0.00	0.00	0.00	0.00	0.16	0.00	0.00
Mn	0.03	0.03	0.03	0.03	0.01	0.02	0.04	0.04	0.62	0.03	0.07
Fe	0.70	0.56	0.68	0.55	0.57	0.47	0.79	0.66	4.43	1.32	1.28
Na	0.02	0.02	0.02	0.02	0.03	0.03	0.04	0.05	–	0.00	0.00
K	0.00	0.00	0.00	0.00	0.04	0.08	0.00	0.01	–	0.00	0.00
Zn	–	–	–	–	–	–	–	–	–	0.08	0.03
Total:	11.00	11.01	11.01	11.02	11.03	11.04	11.06	11.06	15.98	14.61	14.62
A:	0.51	0.51	0.52	0.52	0.51	0.51	0.51	0.51	0.25	0.70	0.72
F:	0.37	0.29	0.36	0.29	0.30	0.26	0.40	0.34	0.85	0.73	0.74
M:	0.63	0.71	0.64	0.71	0.70	0.74	0.60	0.66	0.15	0.27	0.26

Characteristic EMP analyses of old cordierite, recrystallized cordierite, garnet, and staurolite. Cordierite and garnet were analysed using the wavelength-dispersive mode, and staurolite was analysed using the energy-dispersive mode.

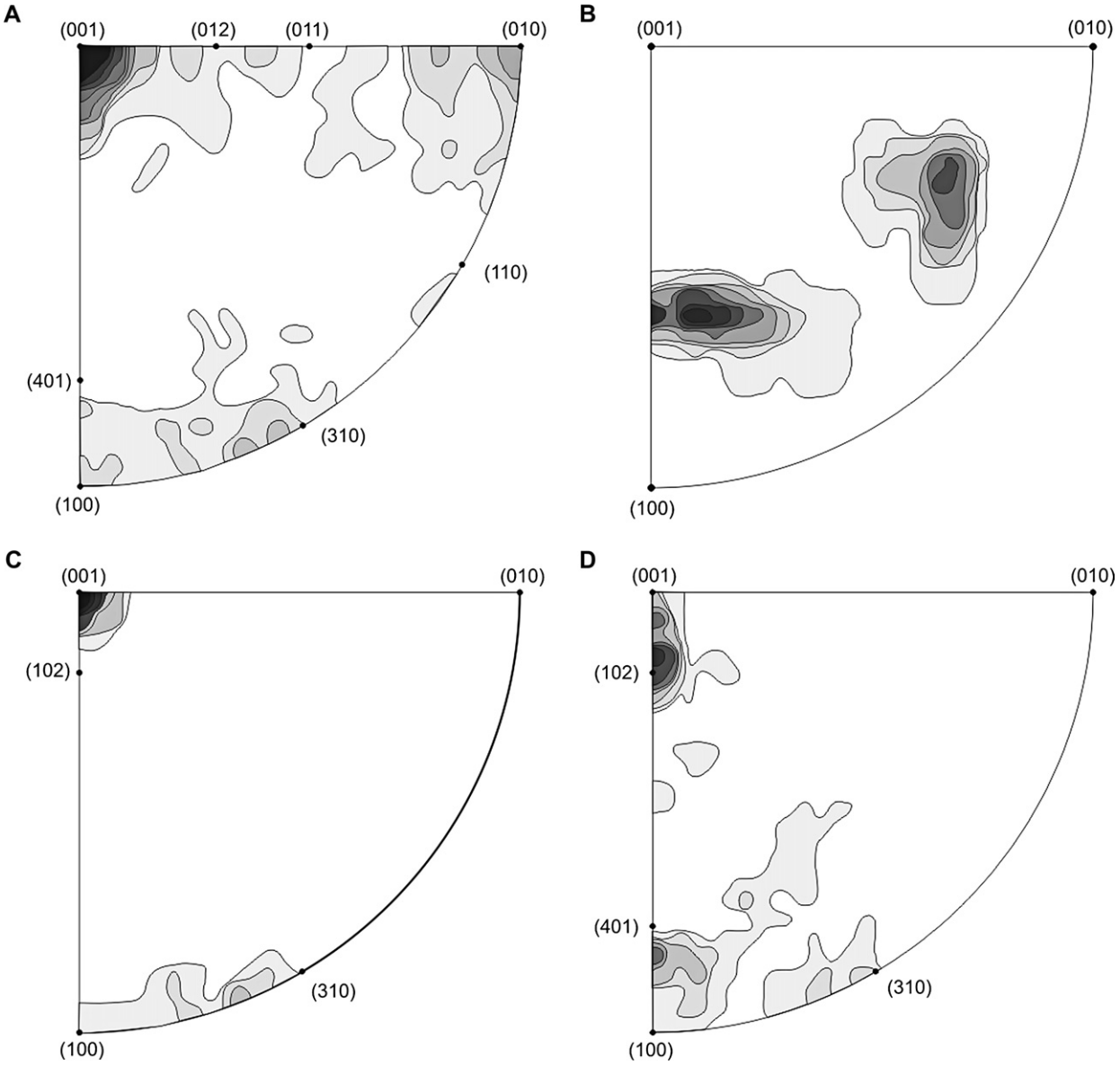

Fig. 3. Crystallographic orientations of subgrain boundary segments from mm-large cordierite host grains, represented as frequency distributions in inverse pole figures. The subgrain boundaries are presented in relation to only one of the neighbouring grains because the crystallographic orientations of the measured subgrains differ only by a few degrees. Sample 'Cafayate', section A1 and A3; equal-area projection, lower hemisphere. (A) Subgrain boundaries from 4 host grains, including measurements presented in C and D; measurements $n = 250$, contour interval ci = 1 multiple uniform distribution [m.u.d.]. (B) Thin-section normals from sample 'Cafayate', section A1 and A3, in relation to parts of cordierite crystals used for measurements presented in A, C and D; $n = 88$; ci = 2 [m.u.d]. (C) Subgrain boundaries away from a zone of recrystallized grains (Fig. 5); $n = 41$, ci = 5 [m.u.d.]; region of non-measurability around the (010) normal. (D) Subgrain boundaries close to a zone of recrystallized grains (Fig. 5); $n = 47$, ci = 2 [m.u.d.]; region of non-measurability around the (010) normal.

and between the zones {100}, {010}, and {001} are absent and they are rare between (310) and (110). Although the measured old cordierite crystals are not randomly oriented (Fig. 3D), all parts of the inverse pole figure are covered by measurements (Fig. 4), however, in diverse frequency. Particularly, the regions close to (010) and (100) have a low probability of measurability, whereas the region close to (001) has a high one, roughly twice as high as the regions close to (010) and (100). Consequently, the (001) maximum of subgrain boundary orientations (Fig. 3C) is too high and the (010) and (100) maxima are too low. Probably, the three maxima have approximately the same population density.

In zones of the cordierite crystals, away from recrystallized grains and typically characterized by a low degree of internal crystal rotation, the subgrain boundaries preferentially form a chessboard pattern (Fig. 2C). By contrast, in zones close to recrystallized grains, characterized by a high degree of internal crystal rotation, the subgrain boundaries show a larger variety of crystallographic orientations (Fig. 5). In the example presented in Fig. 6, the subgrains away from the region of recrystallized grains have two maxima of subgrain-boundary orientations (Fig. 6B), one exactly parallel to (001) and the other sub-parallel to (100). Moreover, subgrain-boundary orientations also occur in the zone {001} between (100) and

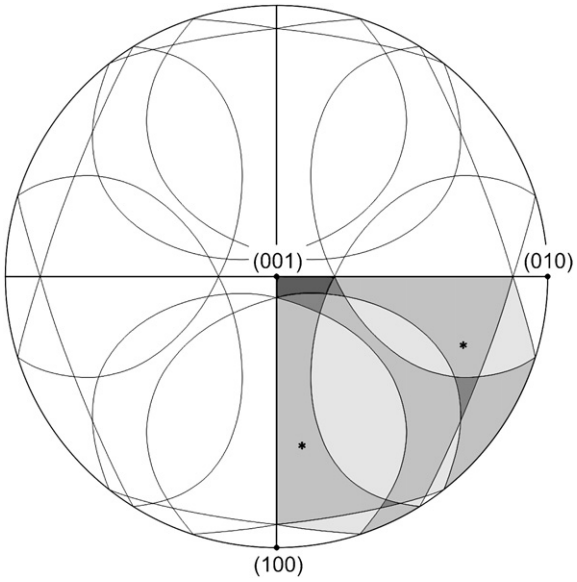

Fig. 4. Probability of subgrain-boundary measurements, based on the two maxima of thin-section normal (Fig. 3B; asterisks). 45° regions of non-measurability around the two maxima, based on a maximum u-stage rotation angle of 45°, projected into one quarter of the inverse pole figure, add up to regions of four different levels of probability, ranging from 50% (white) over 62.5%, 75% and 87.5% (increasing grey) to 100% (darkest grey).

(310) (Fig. 3C). In general, the chessboard patterns are formed by subgrain boundaries approximately parallel to (100), (010) as well as (001).

In the example presented in Fig. 5 the subgrain-boundary orientations close to the region of recrystallized grains are more variable but form nevertheless maxima close to (001) and (100) (Fig. 6B). However, the subgrain boundaries deviate systematically from (001) and (010) by ~15° against the sense of shearing of the nearby micro shear zone. The inverse pole figure reveals a high population density of subgrain boundaries between (001) and (102), with a maximum around (102), and another one between (100) and (401) (Fig. 3D). In addition, weak sub-maxima occur close to (310) and in the region between (001), (100), and (310).

4.2. Recrystallized grains

Small (~40–200 μm; average ~100 μm), equant to slightly elongate, and microscopically strain-free cordierite grains dominantly occur in the described micro shear zones within old cordierite grains, along their margins and around garnet inclusions in cordierite (Fig. 2A,B,D,I). They are interpreted as the result of static recrystallization. Zones of these recrystallized grains are locally rimmed by zones of intense polygonization, but the transition between old and recrystallized grains is commonly sharp, lacking a zone of progressively rotated subgrains. The misorientation between neighbouring subgrains and recrystallized grains is high (up to 50°) and the recrystallized grains are significantly larger than the neighbouring subgrains (Fig. 2A,B,D).

Grain boundaries between recrystallized as well as old and recrystallized grains are straight, but segmented. They only show a weak crystallographic preferred orientation (Fig. 7), in contrast to the subgrain boundaries. Only broad small-circle concentrations around (010) and (001) exist, with maxima away from (001) and (010), and a relatively low population density at (001) and (010). However, the low population density at (100) may result from the preferred orientation of the recrystallized grains, with (100) favourably sub-parallel to the thin-section plane.

4.3. Micro shear zones

Two sets of conjugate shear zones at angles of approximately 50–80° to each other—with σ1 in the obtuse angle—transect several old cordierite crystals, but also occur between cordierite, K-feldspar, and plagioclase grains, and appear to continue as parallel micro-fractures into garnet (Fig. 1). They represent the dominant deformation feature in the studied sample.

Within cordierite, the shear zones are characterized by locally asymmetric zones of (i) aligned biotite, magnetite, and fibrous sillimanite (centre) and recrystallized cordierite (margin) (Fig. 2A,J); (ii) recrystallized cordierite (centre) and cordierite subgrains (margin), with generally sharp boundaries between both regions (Fig. 2A); and (iii) zones of intense polygonization. Terminations of micro shear zones within in old cordierite grains are characterized by zones of recrystallization, grading into zones of intense and/or weak polygonization (Fig. 2A,D). Along micro shear zones, zones of intense polygonization may alternate with zones of recrystallization.

Where the micro shear zones terminate at grain boundaries of cordierite in contact with quartz, quartz forms ~70–1000 μm large grains (Fig. 2I). The smaller quartz crystals are polygonal, the larger crystals show strongly sutured grain boundaries and polygonization.

Micro shear zones between coarse-grained cordierite, K-feldspar, and plagioclase grains are characterized by strongly aligned fibrous sillimanite, fine-grained biotite, and recrystallized grains of cordierite, quartz, plagioclase, and K-feldspar. Commonly, K-feldspar is marginally altered to myrmekite. In few cases, close to the former K-feldspar rim, i.e., close to the micro shear zone, plagioclase of the myrmekites is polygonized, or the myrmekite is partly replaced by a mixture of polygonal plagioclase (~30–100 μm) with quartz grains (~30–60 μm) at plagioclase grain boundary triple junctions (Fig. 2G). In agreement with Hanmer (1982), Vernon et al. (1983), and Vernon (1991), we interpret this texture as a result of myrmekite recrystallization.

The orientation of the shear plane is reflected by strongly aligned biotite from the core of the micro shear zones. The maxima of the biotite basal plane orientation from the two sets of shear zones allow determining their intersection line, i.e. the rotation axis of shear, and the shear direction (oriented in the shear plane, perpendicular to the rotation axis). For one of the micro shear zones the shear direction is confirmed by a quartz-[c] girdle perpendicular to the shear plane and parallel to the rotation axis of shear (Fig. 8). Sense of shearing is

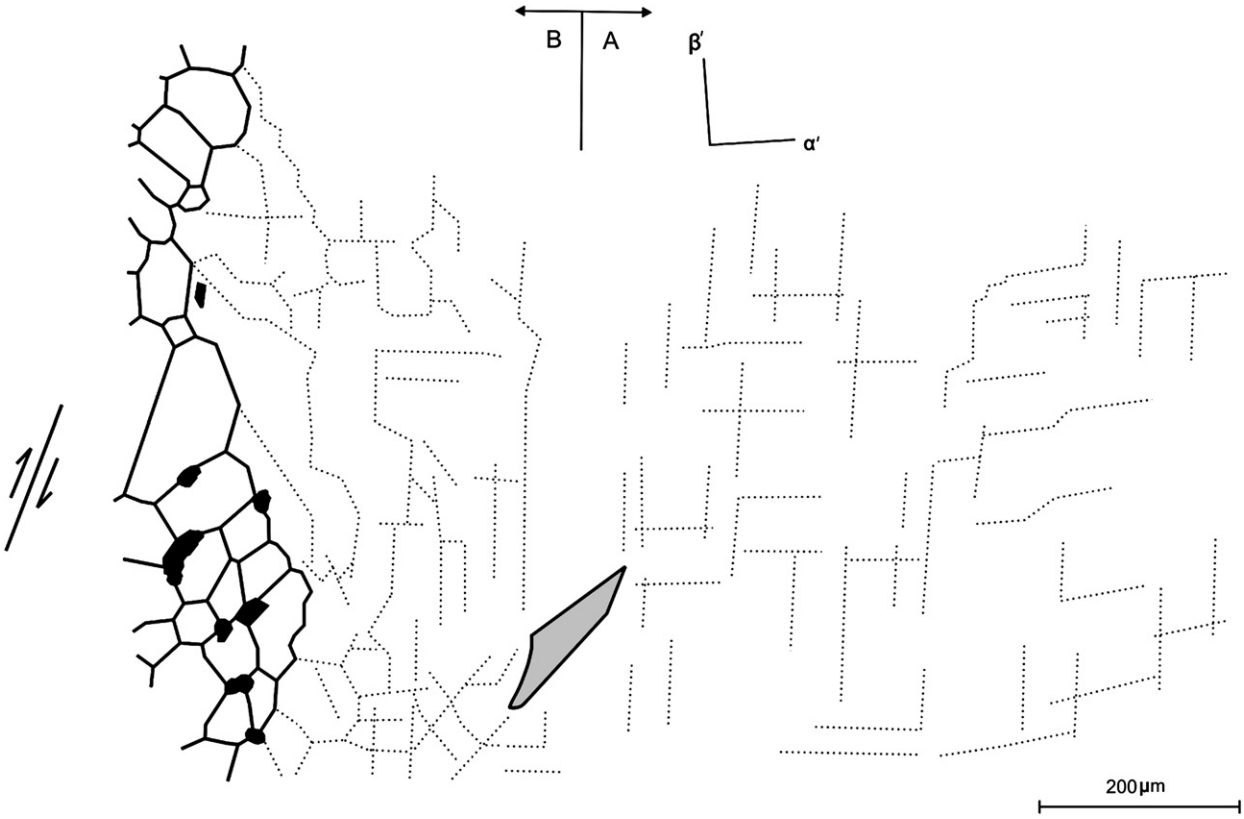

Fig. 5. Thin-section sketch from a polygonized and recrystallized region of a large old cordierite grain; sample 'Cafayate', section A3. Solid lines: high-angle boundaries; dotted lines: low-angle boundaries; bold line with half arrows: approximate orientation and sense of shear of micro shear zone partly represented by the zone of recrystallized grains; grey: biotite; black: opaques. The indicatrix orientations (α', β') of the middle part of the polygonized zone are indicated. Note the change in subgrain-boundary patterns from region A to region B. The subgrain boundary orientations of regions A and B in relation to (001), (010) and (100) are presented in Fig. 3C,D and Fig. 6.

defined by the curvature of biotite and fibrous sillimanite towards the centre of the shear zones and by the orientation of elongate, recrystallized cordierite grains oblique to the shear zones (Fig. 2A,B,J).

4.4. Recrystallized grains within micro shear zones

Based on one sinistral and one dextral (in relation to the thin section) shear zone, the crystallographic orientations of recrystallized grains are described in relation to the kinematic framework. The recrystallized cordierite grains of the sinistral shear zone have a strong crystallographic preferred orientation with incomplete (001) and (010) girdles perpendicular and a strong (100) maximum parallel to the rotation axis of shear (Fig. 9A). (001) and (010) are oriented at angles from ~0° to ~90° to the plane of the shear zone, with broad maxima at ~50°and ~30° (001) of the host grain is sub-parallel and (010) is sub-perpendicular to the shear plane. The two planes differ by ~20–90° from (001) and (010) of the recrystallized grains, roughly on a great circle around the rotation axis of shear and against the sense of sinistral shearing. The two (100) maxima of the host grain are oriented at angles of ~40° and ~5° to the (100) maximum of the recrystallized grains and to the shear plane. The inverse pole figure of the shear direction shows in more detail the relationship between shear direction and crystallography of the recrystallized cordierite grains (Fig. 10A). The shear direction is preferentially oriented in the zone {100}. However, no significant maxima at (001), (010) or at any other low-index direction in the {100} zone occur, except for a broad, slightly increased density around (011).

The recrystallized grains from the dextral shear zone have only a weak crystallographic preferred orientation (Fig. 9B). (001) forms a diffuse half small-circle around the rotation axis of shear, and includes the (001) maximum of the host grain. The half small circle has an opening angle of ~120° and two maxima close to the shear plane. The two (001) maxima of the host grain are located close to the 'beginning' of the half small-circle, in the sense of shearing. (100) of the recrystallized grains, too, forms a diffuse half small-circle around the rotation axis of shear, with an opening angle of ~60°. The two (100) maxima of the host grain are located close to the 'beginning' of the half small-circle, in the sense of shear. (010) of the recrystallized grains forms a diffuse great-circle around the rotation axis of shear, with a maximum perpendicular to the shear plane. The two (010) maxima of the host grain are located close to the 'beginning' of the great-circle, in the sense of shearing, and differ with an angle of ~25° from the (010) maximum of the recrystallized grains. The inverse pole figure (Fig. 10B) exhibits a more or less random distribution of shear direction in relation to the recrystallized

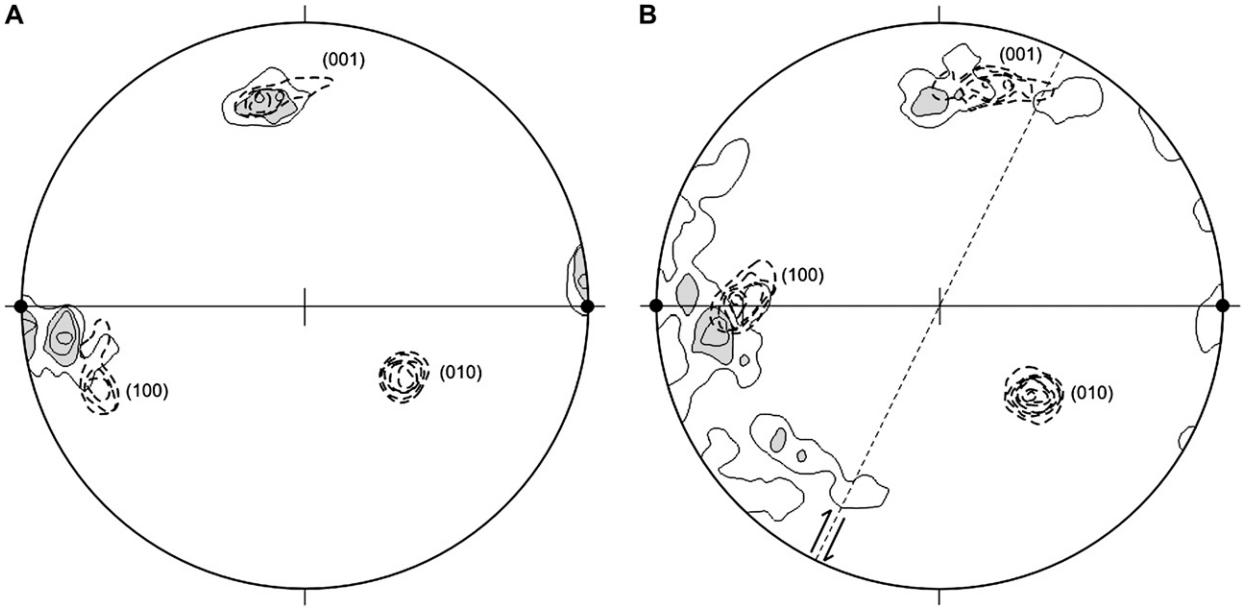

Fig. 6. Orientations of subgrain boundaries and the principal crystallographic planes from a polygonized old cordierite grain. Sample 'Cafayate', section A3; equal-area projection; lower hemisphere; contours = 10 [m.u.d.], broken lines: isolines of population density of the three principal crystallographic directions, solid lines: isolines of population density of subgrain-boundary orientations. (A) Region A as shown in Fig. 5; 41 measurements of subgrain boundaries and crystallographic planes. (B) Region B as shown in Fig. 5; 47 measurements of subgrain boundaries and crystallographic planes; bold broken line and half arrows: shear sense and approximate orientation of sinistral micro shear zone.

cordierite grains. Only one maximum parallel to the (010) normal and another one in the zone {001} parallel to an irrational crystallographic orientation are developed.

In summary, along the sinistral as well as the dextral shear zone, recrystallized cordierite grains are rotated in the sense of shearing but without or with only weak relationship between principal crystallographic directions and the kinematic framework of shear. This argues against crystal plasticity during shearing.

4.5. Crystal rotation across a micro shear zone

Crystallographic orientations of subgrains and recrystallized grains have been measured along three profiles across a sinistral shear zone (Figs. 11 and 12). Dominantly, (010) and (001) of the subgrains are rotated, whereas (100) remains in approximately the same position. The tight scattering of (100) and the apparent location of (010) and (001) on a great circle around the (100) maximum indicate that, during shear, the subgrains rotated around the normal to (100), in the sinistral sense of shear. Over a distance of ~200–250 μm from one side ('bottom' in Fig. 11) towards the shear zone, the subgrains are continuously rotated by ~20–35° (between points 1–5, 16–20 and 30–34 in Figs. 11 and 12). Over ~50 μm to the very centre of the shear zone, again, (001) and (010) of the subgrains are rotated by ~20–35° in the sinistral sense of shear (between points 20–22 and 34–35). (001) and (010) orientations of some recrystallized grains are similar to those of the subgrains (points 6, 8, 9). However, other recrystallized grains show a completely different orientation (points 7 and 10) and, generally, most of the (100) directions of the recrystallized grains deviate at least ~15° from (100) of the subgrains (points 8–10 and 37–39). The sinistral rotation of subgrains continues across the centre of the shear zone (points 21–24) but changes to a dextral rotation in the crystal part 'above' the shear zone (points 11–14, 24–28 and 41–43). This probably indicates a local kink in the crystal or the influence of the dextral micro shear zone nearby (Fig. 11).

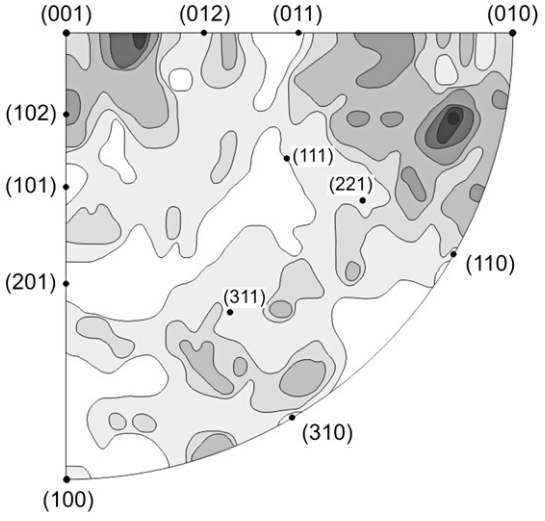

Fig. 7. Crystallographic orientations of grain boundaries of recrystallized cordierite grains from a micro shear zone. The recrystallized grains show a preferred orientation with (100) preferentially parallel to the thin-section plane, which results in a relatively low population density around (100). Sample 'Cafayate', section A1; 322 measurements, based on 161 measured grain boundaries presented in relation to the two neighbouring crystals; inverse pole figure; equal-area projection; contours = 0.5 [m.u.d.].

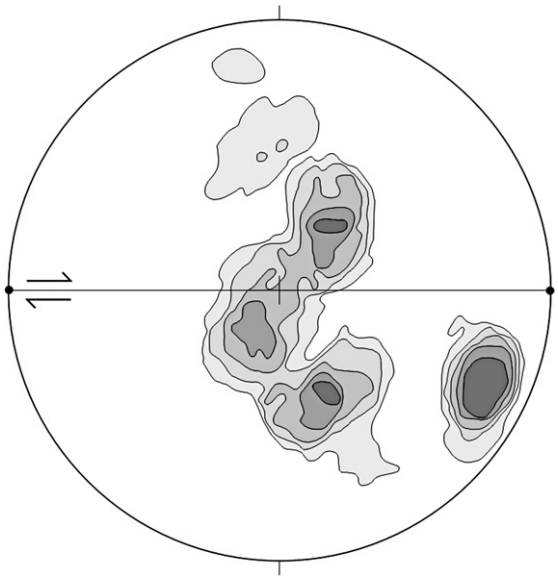

Fig. 8. [c]-axis preferred orientations of recrystallized and annealed quartz from a dextral micro shear zone. Sample 'Cafayate', section A1; 100 measurements; equal-area projection, lower hemisphere; contours = 1.5 [m.u.d.]; half arrows indicate sense of shear. Original measurements have been rotated to a normalized position, i.e., with the shear plane (solid line) vertical E–W and the shear direction (filled circles, determined as direction perpendicular to the intersection line of conjugated shear zones) horizontal E–W. The orientation of the quartz-[c] cross-girdle perpendicular to the constructed shear direction is an additional indication of this direction.

In summary, from the boundary towards the centre of the shear zone, (001) of the subgrains rotates from a position sub-perpendicular to a position sub-parallel to the shear zone and even ~20° beyond. (010) rotates from a position oblique to a position sub-perpendicular to the shear zone, whereas (100) remains in approximately the same position (Fig. 12). This indicates that in polygonized parts of the shear zone crystal rotation was govern by specific glide systems.

5. Mineral chemistry and thermobarometry

Compositionally, old cordierite grains are largely homogeneous in undeformed or weakly deformed crystal domains and away from inclusions of different mineral species, particularly garnet. Significant compositional variations between old and recrystallized cordierite are only seen in their Mg–Fe ratio X_{Mg}. In Sample 'Cafayate' old grains show a uniform X_{Mg} of 0.63–0.64 (Fig. 13A,B). X_{Mg} is significantly higher (0.69–0.73) close to garnet inclusions (Fig. 13A), suggesting Fe–Mg exchange reactions. These values are similar to those from recrystallized cordierite in micro shear zones, which shows an X_{Mg} of 0.66–0.76 (Fig. 13B). There is a tendency towards lower X_{Mg} values ($\leq$0.70) in the centres of larger recrystallized grains. The highest X_{Mg} values of 0.77–0.78 occur in small recrystallized cordierite grains close to garnet (Fig. 13A). The same trend of higher X_{Mg} in recrystallized cordierite compared to old crystal domains is seen in sample 496A (Fig. 13C). Grey-scale variations in SEM backscatter images (Fig. 13C) correlate with these variations in X_{Mg}. Representative compositions of garnet, staurolite, and cordierite are shown in Table 1.

The samples 'Cafayate' and 496A come from the garnet-cordierite-sillimanite zone of the northern Sierra de Quilmes. Cordierite formed at metamorphic peak conditions of 540–630 MPa and 750–800 °C (Büttner et al., 2005). The retrograde regional deformation, commencing at or close to the thermal peak and continuing during slow near-isobaric cooling of the crust, was followed by a post-kinematic equilibration at 380–460 MPa and 500–620 °C (Büttner et al., 2005). The deformation patterns in cordierite are assigned to this retrograde shearing. The conditions at which the deformation in cordierite from sample 'Cafayate' occurred has been determined using petrological methods and temperature-sensitive microfabrics.

In the investigated samples deformation during or close to the metamorphic peak is indicated by (i) chessboard subgrain patterns in quartz away from the micro shear zones, which are interpreted as a result of deformation in the high-quartz field, i.e., at >720 °C at 600 MPa (Kruhl, 1996); (ii) the quartz-[c] orientations from a micro shear zone (Fig. 8), which partly define a single maximum close to the shear direction, indicating dominant prism-[c] glide, characteristic of deformation temperatures above ~700 °C (Blumenfeld et al., 1986; Gapais and Barbarin, 1986; Mainprice et al., 1986); and (iii) by recrystallized plagioclase with average grain diameters of ~500 μm, indicating deformation temperatures of ~720 °C (Kruhl, 2001).

A secondary mineral assemblage consisting of sillimanite, staurolite, magnetite and quartz has formed along the boundaries of recrystallized cordierite (Fig. 13D). Occasionally, staurolite and sillimanite are aligned to the grain boundaries. Non-fibrous alumosilicate in symplectites is most likely kyanite that formed post-kinematically (Büttner et al., 2005). Although the majority of secondary mineral phases is concentrated along grain boundaries of recrystallized cordierite, small randomly oriented sillimanite and staurolite crystals regularly occur within recrystallized cordierite grains (Fig. 13D). The genetic relationship between cordierite recrystallization and the formation of the secondary mineral assemblage at retrograde *P-T* conditions is indicated by (i) the increase of X_{Mg} along grain boundaries of recrystallized cordierite; (ii) the occurrence of the secondary (Fe-rich) mineral assemblage dominantly along grain boundaries of recrystallized cordierite; (iii) the identical composition of undeformed cordierite porphyroclasts close to garnet rims and garnet inclusions and recrystallized cordierite. The secondary assemblage most likely has formed by partial fluid-present cordierite breakdown:

$$\begin{aligned}&\text{low-}X_{Mg}\ \text{cordierite (old)} + \text{fluid}_1\\ &\quad = \text{high-}X_{Mg}\ \text{cordierite (recrystallized)} + \text{staurolite}\\ &\qquad + \text{sillimanite} + \text{quartz} + \text{magnetite} + \text{fluid}_2. \qquad (1)\end{aligned}$$

The composition of phases on the product side of reaction (1), together with garnet rim compositions, has been used for multiphase equilibria *P-T* calculations (TWQ 1.02, Berman, 1991). Average compositions yield an intersection of four independent mineral reactions at 570 °C and 380 MPa. Using single analyses, the calculated *P-T* conditions vary from 360 to 420 MPa

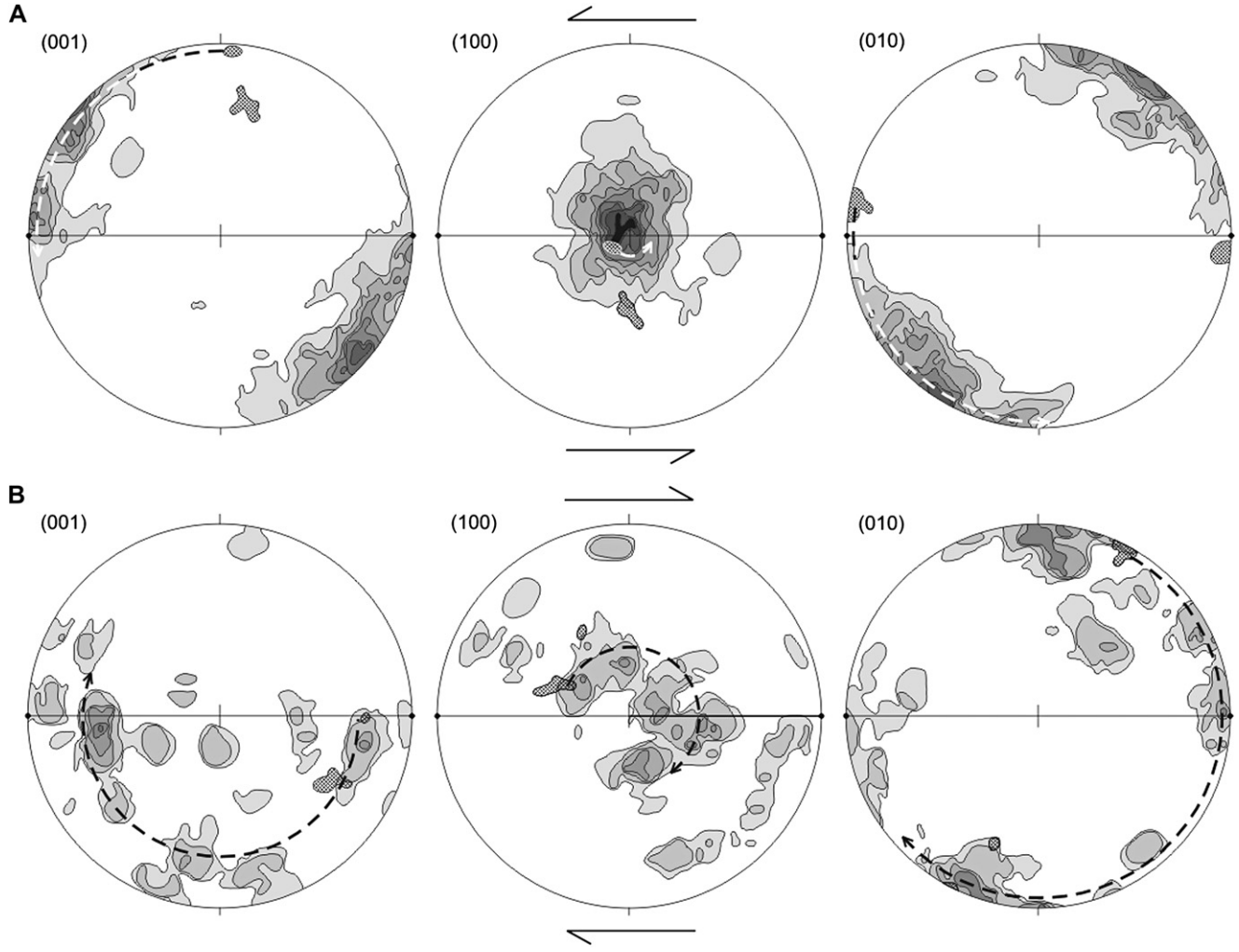

Fig. 9. Crystallographic preferred orientations of the three principal planes of recrystallized cordierite grains in a sinistral and a dextral micro shear zone (Fig. 2A). Original measurements have been rotated to a normalized position, i.e. with the shear plane (solid line) vertical E–W and the shear direction (filled circles, determined as direction perpendicular to the intersection line of conjugated shear zones) horizontal E–W. Equal-area projection, lower hemisphere; contours: 1.5 [m.u.d.]; cross-hatched areas: orientation of several subgrains of the host grain, away from the shear zone; half arrows indicate sense of shear. Sample 'Cafayate', section A1. (A) 168 measurements from a sinistral shear zone. (B) 96 measurements from a dextral shear zone.

and from 555 to 595 °C. We interpret the results from average compositions, and thus ~570 °C and 380 MPa, as the best estimation for the retrograde equilibration subsequent to cordierite recrystallization.

The occurrence of well aligned and randomly oriented secondary staurolite and sillimanite along boundaries of recrystallized cordierite (Fig. 13C,D) suggests that the formation of these minerals has outlasted the deformation. Consequently, the secondary mineral assemblage partly formed during shearing and partly subsequent to shearing. We interpret the inferred temperature of ~570 °C not only as the temperature of retrograde equilibration but also as the temperature during which the micro shear zones formed. Sillimanite, staurolite, and magnetite are concentrated in and aligned parallel to micro shear planes (Fig. 2A,J) as well as randomly oriented along grain boundaries of old and recrystallized cordierite grains (Fig. 2H).

Additional information on temperatures during the formation of the micro shear zones and other related microfabrics is provided by microstructural observations. (i) The recrystallization of plagioclase and K-feldspar points to a minimum temperature of ~500 °C (Voll, 1976; Altenberger et al., 1987; Kruhl, 1993). (ii) The average grain size of statically recrystallized polygonal plagioclase grains is ~60 μm, suggesting a temperature subsequent to recrystallization and coarsening of ~520–550 °C (Kruhl, 2001). However, based on a single data set, the temperature estimation is rather uncertain. (iii) Quartz, recrystallized in the continuation of the micro shear zones, partly shows prismatic subgrain boundaries, suggesting that the formation of the micro shear zones took place within the low-quartz field (Kruhl, 1996) at temperatures below ~660 °C and pressures of ~380 MPa (assuming isobaric cooling below ~700 °C; Büttner et al., 2005, figure 5a). (iv) The quartz-[c] orientation from a micro shear zone defines a dominant girdle perpendicular to the shear direction (Fig. 8), indicating mainly prism-<a> glide characteristic of amphibolite facies deformation (Passchier and Trouw, 2005). (v) Myrmekite may form in a wide range of temperatures,

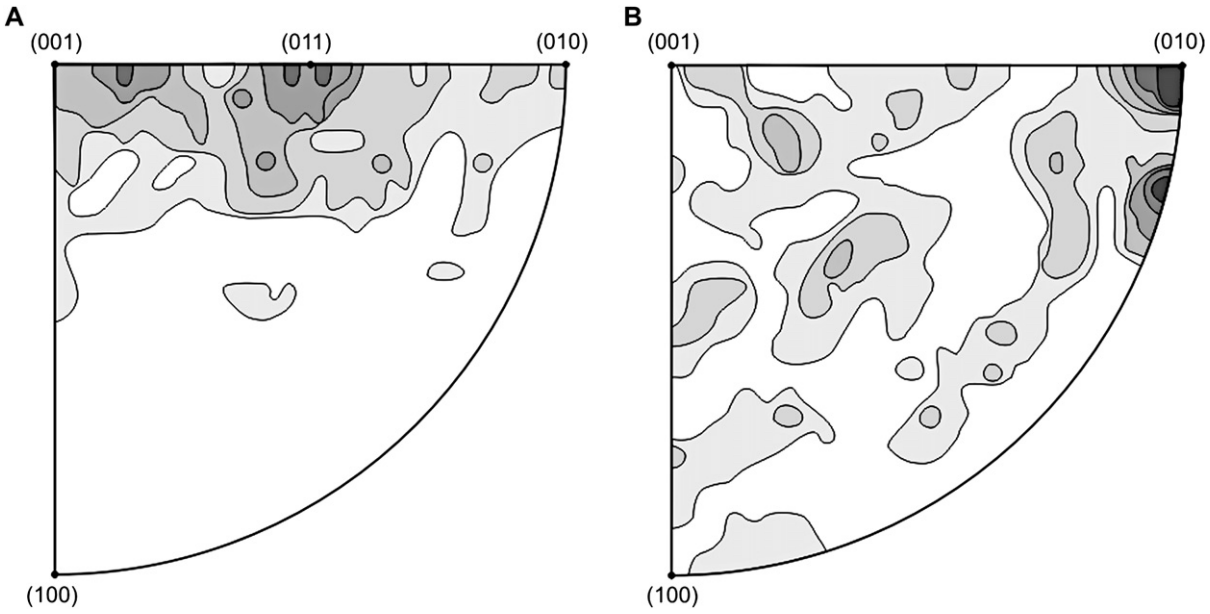

Fig. 10. Orientation of the shear direction in relation to the crystallography of recrystallized grains from a dextral and sinistral micro shear zone (Fig. 2A); the same data as presented in Fig. 9; inverse pole figures, equal-area projection, lower hemisphere; contours = 1.0 [m.u.d.]. A. 168 measurements from a sinistral shear zone. B. 96 measurements from a dextral shear zone.

roughly between 450 °C and 670 °C (Wirth and Voll, 1987; Tribe and D'Lemos, 1996—cited in Vernon 2004, p. 460) and, consequently, myrmekite recrystallization occurred at or below ~670 °C. Even if these microfabric-based temperature estimates may partly not be valid for increased strain rates, they should correctly constrain the conditions at 'normal' strain rates of $\sim 10^{-13}$–10^{-14} [s^{-1}] (Pfiffner and Ramsay, 1982) at the decline of deformation, as shown further below. Except for the rather uncertain plagioclase grain-diameter thermometer, the microfabric-based temperature estimates do not contradict the temperatures inferred from multi-phase equilibria. Therefore, we consider the retrograde equilibration temperature of ~570 °C as the temperature of the shear zone formation and the formation of the related ductile and brittle microfabrics.

6. Discussion

In combination with the *P-T* estimates based on petrological and microstructure-related thermobarometers, the cordierite microfabrics permit (i) to characterize the deformation behaviour of cordierite, and (ii) to constrain the conditions of deformation, during which the micro shear zones and other brittle and ductile microfabrics formed.

6.1. Subgrain boundaries and glide systems

Subgrain boundaries in the cordierite studied have various crystallographic orientations but are dominantly oriented parallel to (001), (010), and (100) (Fig. 3A), where all three orientations have a similar abundance, forming characteristic chessboard patterns. Following the common interpretation that subgrain boundaries develop perpendicular to dominant glide systems (Spry, 1969; Hobbs et al., 1976; Vernon, 2004), the subgrain boundary orientations suggest dominant [001], [010], and [100] glide. The three glide systems seem equivalent and were probably active at the same time. In addition to the three dominant subgrain boundary orientations, subgrain boundaries are relatively abundant in {100}—however, away from low index positions—furthermore suggesting various glide directions perpendicular to [100].

Subgrain boundaries away from the micro shear zones are oriented dominantly parallel to (001), (010) and (100) (Fig. 3C), forming characteristic chessboard patterns. Subgrain boundaries close to and in the micro shear zones have more variable orientations with two significant maxima at an angle of ~15 ° to (001) and (100) in {010} (Fig. 3D). We suggest that the variation in subgrain-boundary orientations close to and in the micro shear zones may result from micro-fracturing and subsequent annealing of the fractures to subgrain boundaries (den Brok and Spiers, 1991; Vernon, 2004, p. 347) or that they indicate additional glide systems active at higher strain rates. The two significant subgrain boundary maxima deviate from (001) and (100) against the sense of shearing (Fig. 6) and, therefore, possibly result from shearing.

Along the micro shear zones, the old cordierite grains are bent and polygonized (Fig. 11). Detailed data from one micro shear zone reveals that, over a distance of ~250–300 μm towards the centre of the shear zone, the crystal is rotated by ~50–60°. The rotation axis is [100], even though [100] differs from the rotation axis of shear by ~40–45° (Fig. 12). (001) of the subgrains rotates from a position sub-perpendicular to a position sub-parallel to the shear zone and (010) rotates from a position oblique to a position sub-perpendicular to the shear zone. Thus, crystal rotation occurs dominantly through

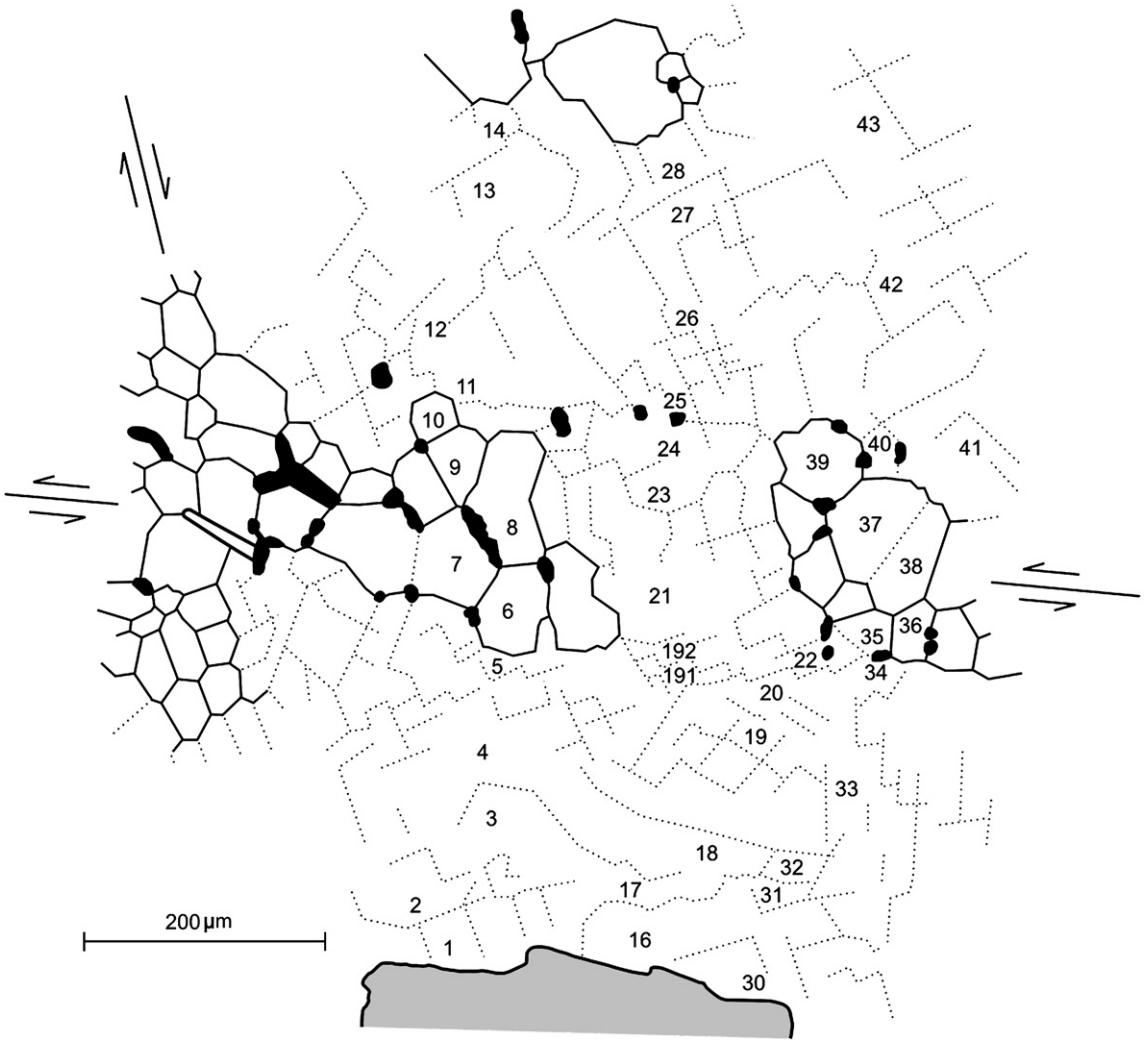

Fig. 11. Thin-section sketch from a polygonized and recrystallized region of a large old cordierite grain; sample 'Cafayate', section A1. Continuous lines: high-angle boundaries; dotted lines: low-angle boundaries (only boundaries with a well visible misfit are shown); bold lines with half arrows: approximate orientation and sense of shear of a dextral and a sinistral micro shear zone, partly represented by the zone of recrystallized grains; grey: garnet; bold outlined needle: sillimanite; black: opaques; numbers: locations of indicatrix measurements, as indicated in Fig. 12A and B.

(001)[010] glide. Along the measured profiles (001) is rotated with up to ~20° beyond parallelism to the micro shear zone. This indicates that (001) is not stabilized in a position parallel to the shear plane to facilitate shearing but that the crystal rotation also occurs through (010)[001] glide and possibly through glide on additional {100} planes under continuing shear. Given that subgrain boundaries parallel (100) are developed in cordierite grains of appropriate orientations, i.e., with (100) perpendicular or sub-perpendicular to the thin-section plane, [100] glide is also assumed to be active during crystal rotation at micro shear zones, in addition to [001] and [010] glide.

To our knowledge, only one other study on subgrain boundary orientations and glide systems in cordierite exists: the study of naturally deformed cordierite by van Roermund and Konert (1990). These authors describe subgrain boundary orientations in cordierite, deformed at ~550–825 °C and 300–500 MPa, as oriented dominantly parallel to (001) and sub-parallel to (010). Based on fabric diagrams and transmission electron microscope observations, they infer dominant (010)[001] glide, assisted by (010)[100] as well as (001)[100] glide. These results are in agreement with the results of the present study, which additionally indicate preferred glide parallel [010].

6.2. Grain boundaries

In contrast to subgrain boundaries of old cordierite grains, the grain boundary orientations of the recrystallized grains show two weak maxima at ~15–20° to (001) and to (010) and (110), and other weak sub-maxima in various irrational crystallographic positions (Fig. 7). These diffuse orientations suggest that the recrystallized grains did not form through subgrain rotation (where orientations of grain boundaries would be similar to the orientation of subgrain boundaries; e.g., for cordierite, van Roermund and Konert, 1990) but through

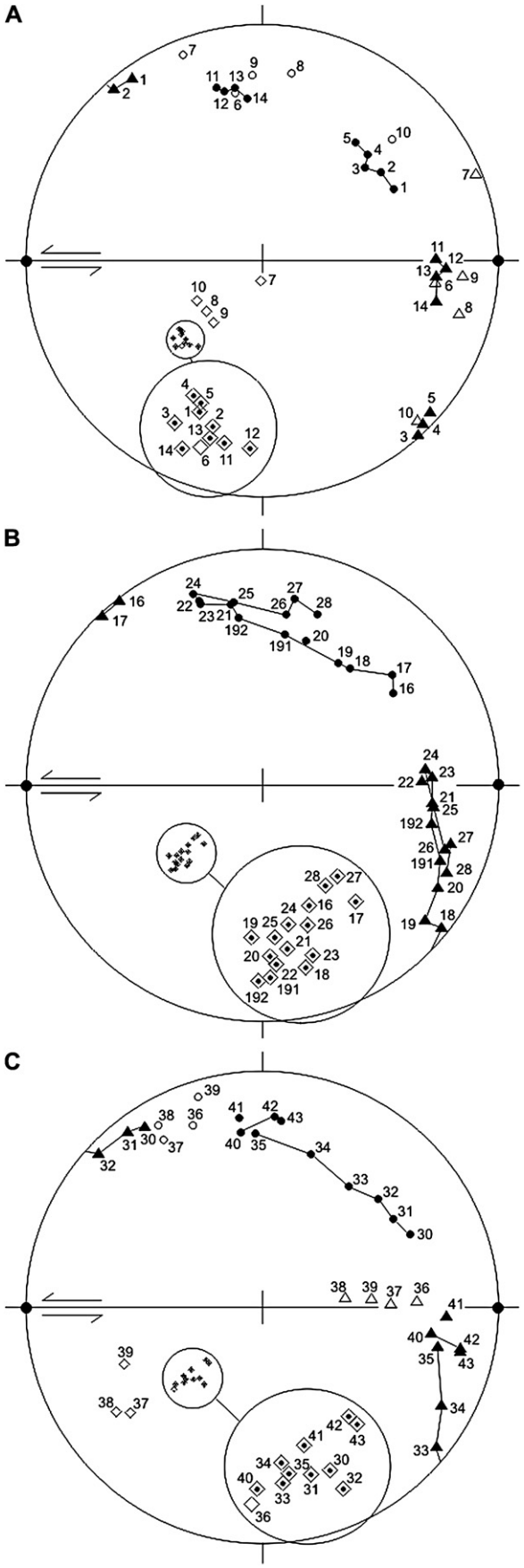

fracturing (see further below), mechanically producing nuclei which subsequently formed recrystallized grains by grain coarsening. For quartz, grain coarsening results in the formation of grain boundaries preferentially oriented in certain high-index or irrational positions (Kruhl, 2001; Kruhl and Peternell, 2002; Kuntcheva et al., 2006) where good match coincidence site lattice orientations are not preferentially occupied and most of the grain boundaries represent general boundaries. Nevertheless, even the high-index or irrational positions represent stable orientations where the grain boundaries are kept during post-deformation migration (Kuntcheva et al., 2006). We would like to suggest that the studied cordierite grain boundaries, too, are crystallographically controlled in a rather complex way and stabilized while migrating during grain coarsening.

6.3. Cordierite rheology

It is established that cordierite shows similar ductile microfabrics as other rock-forming minerals (Vernon, 2004) but not much is known about the rheological behaviour of cordierite at natural strain rates and various temperatures. Recrystallization and the formation of subgrains have been described from upper amphibolite and granulite facies rocks (van Roermund and Kohnert, 1990; Kruhl and Huntemann, 1991; Vernon, 2004, and personal communication), but a lower temperature limit for the recrystallization of cordierite is not known.

Cordierite from this study behaves more ductilely than plagioclase during deformation at medium amphibolite facies conditions. In addition to static recrystallization along shear zones and mechanical twinning, the cordierite is affected by intense polygonization and crystal rotation, whereas plagioclase is only slightly bent and rarely polygonized. These cordierite and plagioclase textures may be evidence for a higher plasticity of cordierite relative to plagioclase during the formation of the subgrains, i.e., at 'normal' strain rates and ~570 °C. However, cordierite may not necessarily recrystallize at lower temperatures than plagioclase. The rigidity of plagioclase in the sample studied may also be a result of the typically high strength of large plagioclase crystals, even above the recrystallization temperature of ~500 °C at 'normal' strain rates (Tullis, 1983; Vernon, 2004). We suggest that cordierite and plagioclase most likely react plastically over a similar temperature range.

Fig. 12. Crystallographic orientations of cordierite subgrains (closed symbols) and recrystallized grains (open symbols) measured along three profiles A, B, and C across a sinistral shear zone. Original measurements have been rotated to a normalized position, i.e., with the shear plane (solid line, half arrows: sense of shear) vertical E–W and the shear direction (filled circles, determined as direction perpendicular to the intersection line of conjugated shear zones) horizontal E–W. The strike of the shear plane was measured in the thin section; the dip versus the thin-section plane and the shear direction were taken from the micro shear zones presented in figures 2A and 9, and, may therefore be slightly uncertain. Circles: indicatrix α = normal to (001), squares: indicatrix β = normal to (100), triangles: indicatrix γ = normal to (010); the solid lines serve to emphasize the spatial sequence of the measurement points; equal-area projection, lower hemisphere; numbers coincide with numbers in Fig. 11.

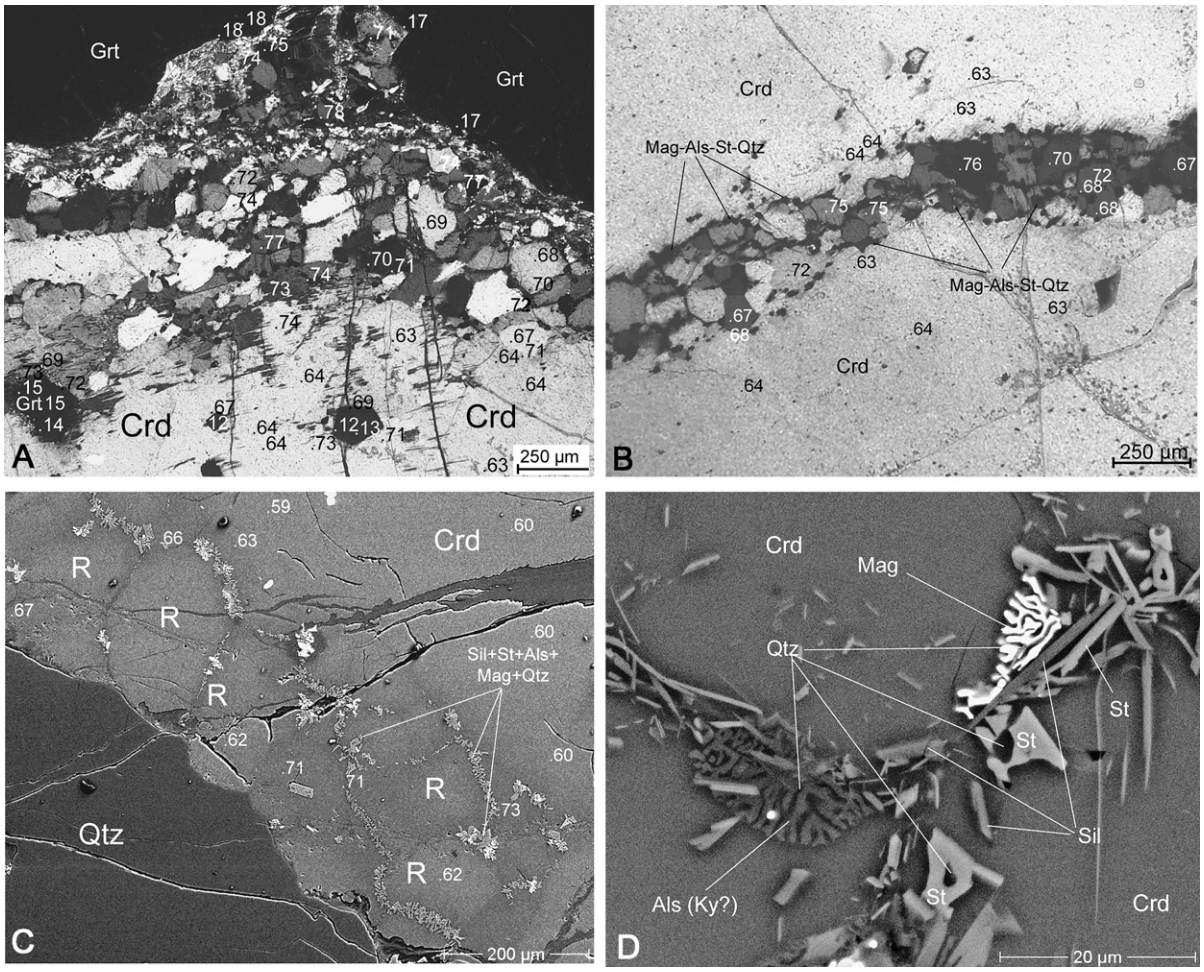

Fig. 13. Photomicrographs and SEM backscatter images of samples 'Cafayate' and 496A. Numbers represent X_{Mg} values in cordierite (Crd) and garnet (Grt). (A) High X_{Mg} values (0.67–0.78) occur in recrystallized cordierite in a micro shear zone and in old cordierite close to garnet inclusions. Significantly lower X_{Mg} values (0.63–0.64) occur within the old cordierite away from garnet; sample 'Cafayate', crossed polarizers. (B) A bimodal distribution of X_{Mg} is developed between recrystallized cordierite in a micro shear zone (0.67–0.76) and in undeformed or less deformed old cordierite (0.63–0.64); sample 'Cafayate', crossed polarizers. (C) The SEM backscatter image shows zonal X_{Mg} composition in recrystallized cordierite grains along the rim of an old cordierite (Crd) from sample 496A. Dark grey colours around grain boundaries of the recrystallized cordierite grains and the newly crystallized assemblage of magnetite (Mag), sillimanite (Sil), staurolite (St), and quartz (Qtz) reflect higher Mg contents relative to core compositions of the old and the recrystallized cordierite grains. Grey-scale variations in cordierite reflect the size of domains affected by diffusion-related mineral reaction. (D) SEM backscatter image of recrystallized cordierite and the secondary mineral assemblage along boundaries of recrystallized cordierite. Sillimanite and staurolite (Sil, St) are well aligned parallel to cordierite grain boundaries. Locally, fine-grained randomly oriented staurolite and sillimanite inclusions in cordierite suggest grain coarsening; sample 'Cafayate'.

6.4. Strain-rate dependent deformation

Our microstructural analysis, combined with thermobarometric estimates, suggests that crystal bending, fracturing and the formation of micro shear zones, subgrains, recrystallized grains, grain boundary sutures, and deformation twins, occurred during one deformation event at highly variable strain rates but at medium amphibolite facies temperatures during the retrograde *P-T* evolution. Fig. 14 schematically summarizes our interpretation of the deformation history and the evolution of the cordierite microfabrics in four stages, discussed in more detail further below: (i) formation of brittle, conjugate micro shear zones and surrounding zones of micro-fractures, producing rotated, fine-grained cordierite crystal fragments at strain rates of $\geq \sim 10^{-7}$ [s^{-1}] and ~570 °C (Stage 1); (ii) circulation of fluids through micro shear zones and micro fractures, thereby oriented growth of sillimanite, staurolite, magnetite, and quartz (in a reaction with low-X_{Mg} cordierite) in shear planes and along micro fractures, and polygonization, i.e., ductile deformation of cordierite at strain rates decreasing from $\geq \sim 10^{-7}$ to ~0 [s^{-1}] and temperatures of ~570 °C (Stage 2); (iii) continuing circulation of fluids, thereby random growth of sillimanite, staurolite, magnetite, and quartz in shear planes and along micro fractures, as well as formation of statically recrystallized cordierite grains, subsequent to deformation at ~570 °C (Stage 3); (iv) coarsening of the statically recrystallized cordierite grains and continuing circulation of fluids, thereby random post-kinematic growth of sillimanite, staurolite, magnetite, and quartz, mainly along grain boundaries of the recrystallized cordierite grains, still at ~570 °C (Stage 4). Of course, the subsequent evolutionary stages, e.g. the formation of fractures and the infiltration of

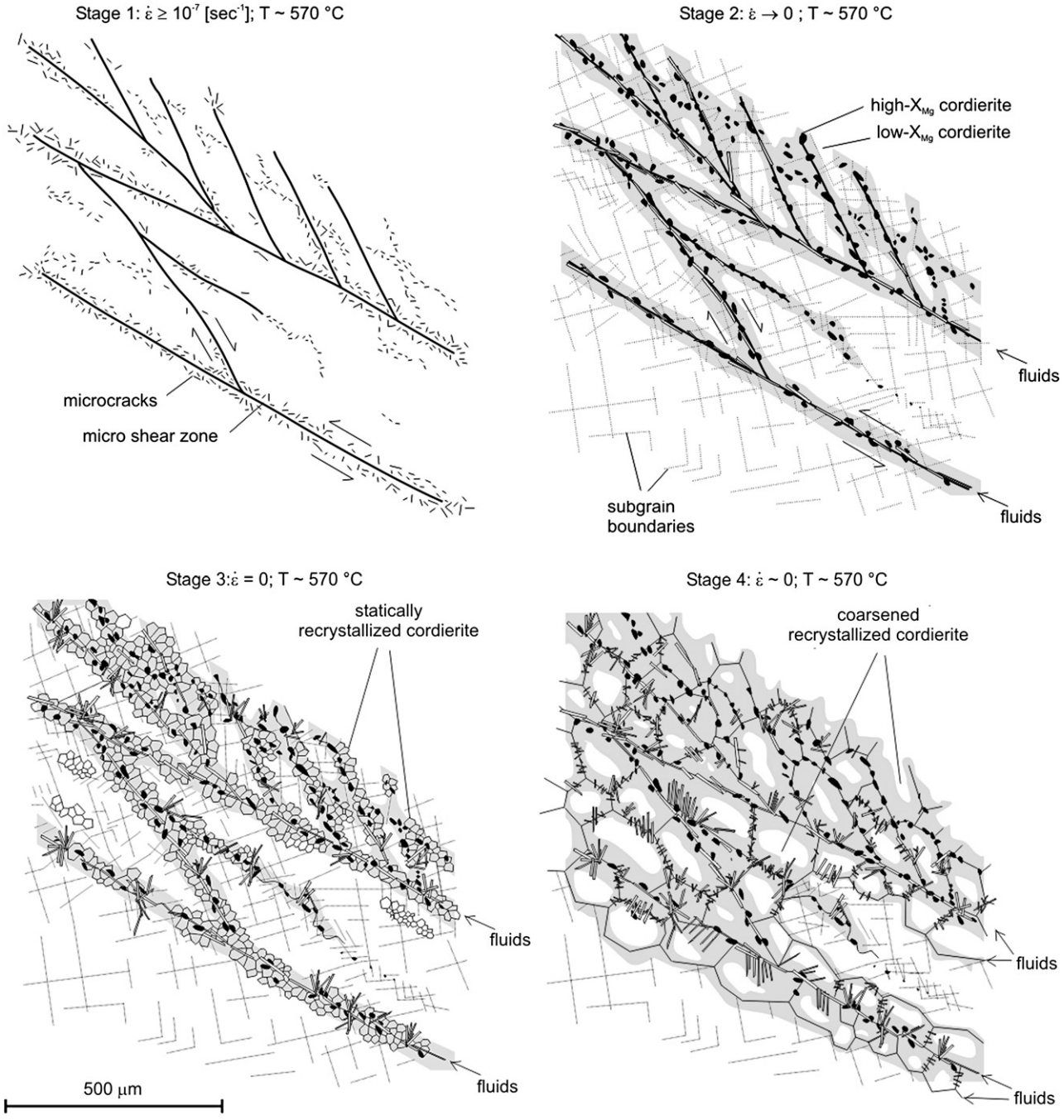

Fig. 14. Model for the development of the studied micro shear zones and related microfabrics. The schematic sketches illustrate four stages of different deformation and fluid infiltration/reaction conditions. See text for details.

fluids, may overlap to a more or less large extend and may be coeval in different parts of the rock. The following observations are evidence for the inferred evolution.

6.4.1. Stage 1

(i) Petrological and microstructure-based thermometers, in combination with the cordierite microfabrics, permit to constrain that deformation along the micro shear zones was active at ~570 °C, a temperature at which at least quartz and feldspar, but probably also cordierite, are ductile. Although the *P-T* relevant assemblage of sillimanite, staurolite, magnetite, and quartz was not present during Stage 1, we assume that the temperature during the formation of the micro cracks was similar or even higher than 570°, given that the time between the formation of the micro cracks and the infiltration of fluids along the micro cracks should have been geologically short (otherwise the micro cracks would have healed). Assuming that not only cordierite and feldspar, but also quartz, were deformed under brittle conditions, a minimum strain rate of $\sim 10^{-7}$ [s^{-1}] can be calculated, using the strain-rate and temperature dependent brittle-ductile transition of quartz, determined in experiments and nature (Fig. 15).

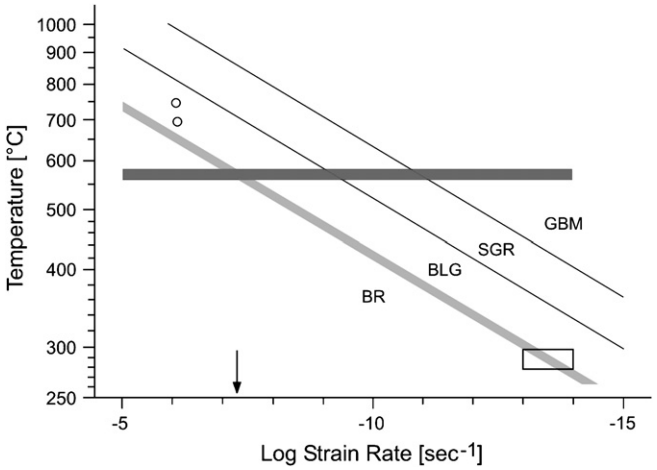

Fig. 15. Temperature versus strain rate in a double-logarithmic diagram illustrating the fields of brittle deformation (BR), and of dominant bulging recrystallization (BLG), subgrain rotation recrystallization (SGR), and grain boundary migration recrystallization (GBM) of quartz. The approximate beginning of quartz recrystallization (light grey stripe) with increasing temperature and decreasing strain rate is constructed on the basis of (i) quartz recrystallization temperature at 'normal' strain rates (box—after Voll, 1976; van Daalen et al., 1999; Stöckhert et al., 1999; Stipp et al., 2002a), (ii) beginning of recrystallization in experiments (circles—Hirth and Tullis, 1992, modified in Stipp et al., 2002b), and (iii) the assumption that the beginning of recrystallization is linear in a log–log plot of temperature versus strain rate and approximately parallel to transitions between the different fields of dominant recrystallization mechanisms (after Stipp et al., 2002b). The dark grey stripe indicates the deformation temperature of ~570 °C during formation of micro shear zones and related microfabrics, which demonstrates a brittle-ductile transition of quartz at a minimum strain rate of $\sim 10^{-7}$ (s^{-1}) (arrow).

(ii) The micro shear zones occur in all rock-forming minerals (cordierite, K-feldspar, plagioclase, quartz—with the possible exception of garnet). At least quartz and feldspar have different rheological properties at the inferred medium amphibolite facies temperatures (Tullis, 1983). But even in places where the more ductile quartz is modally dominant in the sample the strain is not concentrated in quartz, as it is typically the case for amphibolite facies shear zones (e.g., Altenberger and Kruhl, 2000; Vernon, 2004).

(iii) Locally, large fragments of former single cordierite grains are displaced along thin zones of polygonization and recrystallization, enriched in sillimanite and opaques (staurolite, magnetite, quartz) (Fig. 2I). Most likely, these zones represent annealed fractures. In addition, quartz in the continuation of the shear zones in cordierite forms large, polygonal, strain-free grains (Fig. 2I), thus indicating the absence of dynamic recrystallization and, consequently, the absence of a larger amount of ductile deformation during formation of the shear zones.

(iv) No evidence exists that the micro shear zones cross cut other deformation textures, such as recrystallized grains, or deformation twins in old cordierite grains. This indicates that they predate these textures.

(v) Along the shear zones, the principal crystallographic planes of the recrystallized cordierite grains are rotated in the sense of shear and against the crystallographic planes of the adjacent old cordierite grains. Independent from any potential glide systems, the rotation occurs around the axis of shear (Fig. 9), suggesting mechanical rotation of small crystal fragments. These fragments form the nuclei of the statically recrystallized grains subsequently generated by grain coarsening. Possibly, the fluid pressure during the early phase of fluid infiltration (Stage 2) facilitated the mechanical rotation of fragments, as recently suggested for experimentally formed micro shear zones (Vernooij et al., 2006).

6.4.2. Stage 2

(i) Oriented sillimanite and biotite occur in narrow zones in the centre of the inter- and intra-crystalline micro shear zones and in thin shear planes (Fig. 2A,B,J). A fine-grained secondary mineral assemblage including sillimanite and opaques (staurolite, magnetite, quartz) is concentrated in partly irregular planes within old cordierite grains (Fig. 2D,I). Both observations indicate that the *P-T* relevant assemblage formed in a reaction with a fluid during and shortly after the formation of micro shear zones and fractures. This conclusion is supported by the fact that particularly zones characterized by cataclastic deformation may channelize fluids (Vernon 2004, p. 354). We assume that, as a result of fluid infiltration and reaction, the X_{Mg} of cordierite has changed along the shear zones, even though evidence may have been destroyed during later stages of annealing and grain coarsening (stages 3 and 4).

(ii) Along the shear zones, cordierite is characterized by intense polygonization (Fig. 2A,B,D) and crystal rotation (Figs. 11 and 12), as well as a lack of dynamic recrystallization. Since a longer period of strong deformation at conditions of cordierite ductility, i.e., at the given mid-amphibolite facies temperatures and 'normal' strain rates, would lead to dynamic recrystallization the lack of dynamic recrystallization probably indicates a rapid decline of strain rate and, consequently, deformation intensity. In addition, the variation of polygonization across and parallel to the shear zones with respect to intensity and types of subgrain boundaries (Figs. 2A,D and 11), may indicate a spatial variation in deformation intensity and strain rate.

(iii) Subgrain boundaries close to and in the micro shear zones have more variable orientations than subgrain boundaries away from the micro shear zones (Fig. 3C,D). This variation is probably the result of more variable glide systems at increased strain rates and/or of microfracturing during increased strain rates and subsequent annealing of the microfractures during decreased strain rates, forming subgrain boundaries.

6.4.3. Stage 3

(i) Along the micro shear zones cordierite is only statically but not dynamically recrystallized (Fig. 2A,B). Based on the regional *P-T-d* development (Büttner et al., 2005), for the formation of the recrystallized cordierite grains studied, annealing in the ductile field, subsequent to deformation in the brittle field, can be ruled out as a driving mechanism. We suggest that a strain-rate decrease to zero, at constant temperatures of ~570 °C, permitted static recrystallization.

(ii) Given that (a) grain boundary migration is a geologically rapid process (Voll, 1960; Urai, 1983; Urai et al., 1986; Mancktelow and Pennacchioni, 2004) which should immediately start after strain rates/temperatures appropriate for

grain boundary migration are reached, and (b) the recrystallized cordierite grains, overprinting the Stage 2 subgrain patterns, as well as recrystallized plagioclase and quartz grains are strain free, a geologically fast decline of the strain rate to zero is suggested. If deformation at 'normal' strain rates would have been active over an extended period of time at temperatures of ~570 °C indications of dynamic recrystallization should be observed, but they are not.

(iii) Randomly oriented sillimanite and opaques (staurolite, magnetite, quartz) along the micro shear zones are evidence for post-kinematic fluid infiltration and for reaction between fluid and cordierite.

6.4.4. Stage 4

(i) Eventually, grain boundary migration and coarsening of the statically recrystallized cordierite grains, indicated by occasional, randomly oriented inclusions of secondary sillimanite and staurolite, ceased in contact to opaques (staurolite, magnetite, quartz) massively occurring along the former shear planes (Fig. 2B,E,J). Here, migrating boundaries were pinned and possibly stopped by crystallographically controlled grain boundary equilibration (Kruhl, 2001; Kuntcheva et al., 2006).

(ii) Randomly oriented sillimanite, staurolite, magnetite, and quartz along grain boundaries of recrystallized and old cordierite grains are evidence for continuous fluid infiltration during the last stage of fabric development and for a reaction between fluid and cordierite, leading to a compositional change along the grain boundaries. The random orientation of the reaction products indicates that deformation was negligible to absent at this time.

The significant strain rate variation within a geologically short period of time suggests that the sets of conjugate micro shear zones formed in a paleo-seismic event, and, therefore, may help to infer the orientation of paleo-stress fields. Typically, pseudotachylites are taken as evidence for paleo-seismic events (Sibson, 1975). However, the advantage of using conjugate brittle shear zones, developed in a generally ductile regime, is that (i) these shear zones are not limited to specific lithologies and (ii) determining the paleo-stress orientation is more straightforward. Moreover, analysing the different brittle-ductile behaviour of various minerals may permit a better constraint of strain rates during paleo-seismic events (Ellis and Stöckhert, 2004).

As discussed by Vernon (2004, p. 347), there are numerous natural as well as experimental examples, showing brittle precursors of recrystallized grains and the importance of brittle deformation and the interaction between brittle and ductile processes for rock deformation (Tullis and Yund, 1987; Nyman et al., 1992; den Brok, 1992; den Brok et al., 1998; McLaren and Pryor, 2001). A recent investigation on micro shear zones, experimentally produced in quartz (Vernooij et al., 2006), shows a strong resemblance of microstructures to those investigated in the present study and a strong similarity of shear zone development. This similarity, again, suggests that such development, transitional between brittle and ductile, may represent a common type of deformation behaviour of crystalline material. In addition, our study confirms the importance of brittle deformation and shows that the analysis of the interaction of brittle and ductile deformation may provide detailed information on strain rates and paleo-stress fields. Although some microfabrics have a 'short memory' of their origin (Means, 1989) combined petrological and microstructural studies—particularly if crystallographic preferred orientations and microstructure-based thermometry are included—may reveal a complex deformation history of a rock.

Acknowledgements

During winter 2003/2004, universal-stage measurements were performed at the Technical University of München and EMPA analytics at the Rhodes University Grahamstown. We thank Djordje Grujic for helpful comments, Friedrich Lucassen for providing the samples studied, Gerhard Franz for initial discussions and support of this study within the Special Research Program 'SFB 267: Deformation Processes in the Andes', Constanze von Engelhardt for the polished thin sections, and Klaus Haas for help with the figures. Ulrich Gernert (TU Berlin) has helped with the SEM imaging and EDS analytics. Siksha Bramedo is thanked for technical assistance in EMPA analytics at Rhodes University. Jörn H. Kruhl acknowledges the hospitality of the Departments of Geography and Geology at Saint Mary's University, Halifax, while working on the manuscript. Saskia Erdmann acknowledges the support of a Killam Scholarship at Dalhousie University. The two anonymous referees are thanked for their reviews.

References

Altenberger, U., Hamm, N., Kruhl, J.H., 1987. Movements and metamorphism north of the Insubric Line between Val Loana and Val d'Ossola, N. Italy. Jahrbuch der Geologischen Bundesanstalt Wien 130, 365–374.

Altenberger, U., Kruhl, J.H., 2000. Dry high-temperature shearing in the fossil Hercynian lower crust of Calabria (S. Italy). Periodico di Mineralogia 69, 125–142.

Blumenfeld, P., Mainprice, D., Bouchez, J.-L., 1986. C-slip in quartz from subsolidus deformed granite. Tectonophysics 127, 97–115.

Büttner, S.H., Glodny, J., Lucassen, F., Wemmer, K., Erdmann, S., Handler, R., Franz, G., 2005. Ordivician metamorphism and plutonism in the Sierra de Quilmes metamorphic complex: implications for the tectonic setting of the northern Sierras Pampeanas (NW Argentina). Lithos 83, 143–181.

den Brok, S.W.J., 1992. An experimental investigation into the effect of water on the flow of quartzite. Geologica Ultraiectina 95, 178.

den Brok, S.W.J., Spiers, C.J., 1991. Experimental evidence for water weakening of quartzite by microcracking plus solution-precipitation creep. Journal of the Geological Society of London 147, 541–548.

den Brok, S.W.J., Zahid, M., Passchier, C.W., 1998. Cataclastic solution creep of very soluble brittle salt as a rock analogue. Earth and Planetary Science Letters 163, 83–95.

Ellis, S., Stöckhert, B., 2004. Elevated stresses and creep rates beneath the brittle-ductile transition caused by seismic faulting in the upper crust. Journal of Geophysical Research 109, B05407.

Gapais, D., Barbarin, B., 1986. Quartz fabric transition in a cooling syntectonic granite (Hermitage Massif, France). Tectonophysics 125, 357–370.

Gibbs, G.V., 1966. The polymorphism of cordierite I: The crystal structure of low cordierite. The American Mineralogist 51, 1068–1987.

Hanmer, S., 1982. Microstructure and geochemistry of plagioclase and microcline in naturally deformed granite. Journal of Structural Geology 4, 197–214.

Hirth, G., Tullis, J., 1992. Dislocation creep regimes in quartz aggregates. Journal of Structural Geology 14, 145–159.

Hobbs, B.E., Means, W.D., Williams, P.F., 1976. An outline of structural geology. John Wiley and Sons, New York.

Holdaway, M.J., Lee, S.M., 1977. Fe-Mg cordierite stability in high-grade pelitic rocks based on experimental, theoretical and natural observations. Contributions to Mineralogy and Petrology 63, 175–198.

Kruhl, J.H., 1993. The *P-T*-d development at the basement-cover boundary in the north-eastern Tauern Window (Eastern Alps): Alpine continental collision. Journal of metamorphic Geology 11, 31–47.

Kruhl, J.H., 1996. Prism- and basis-parallel subgrain boundaries in quartz: a micro-structural geothermobarometer. Journal of metamorphic Geology 14, 581–589.

Kruhl, J.H., 2001. Crystallographic control on the development of foam textures in quartz, plagioclase and analogue material. International Journal of Earth Sciences 90, 104–117.

Kruhl, J.H., Huntemann, T., 1991. The structural state of the former lower continental crust in Calabria (S. Italy). Geologische Rundschau 80, 289–302.

Kruhl, J.H., Peternell, M., 2002. The equilibration of high-angle grain boundaries in dynamically recrystallized quartz: the effect of crystallography and temperature. Journal of Structural Geology 24, 1125–1137.

Kuntcheva, B.T., Kruhl, J.H., Kunze, K., 2006. Crystallographic orientations of high-angle grain boundaries in dynamically recrystallized quartz: first results. Tectonophysics 421, 331–346.

Mainprice, D., Bouchez, J.-L., Blumenfeld, P., Tubià, J.M., 1986. Dominant c-slip in naturally deformed quartz: implications for dramatic plastic softening at high temperature. Geology 14, 819–822.

Mancktelow, N.S., Pennacchioni, G., 2004. The influence of grain boundary fluids on the microstructure of quartz-feldspar mylonites. Journal of Structural Geology 26, 47–69.

McLaren, A.C., Pryor, L.L., 2001. Microstructural investigation of the interaction and interdependence of cataclastic and plastic mechanisms in feldspar crystals deformed in the semi-brittle field. In: Boland, J., Ord, A. (Eds.), Deformation Processes in the Earth's Crust. Tectonophysics 335, pp. 1–15.

Means, W.D., 1989. Synkinematic microscopy of transparent polycrystal. Journal of Structural Geology 11, 163–174.

Nyman, M.W., Law, R.D., Smelik, E.A., 1992. Cataclastic deformation mechanism for the development of core-mantle structures in amphibole. Geology 20, 455–458.

Passchier, C.W., Trouw, R.A.J., 2005. Microtectonics, second ed. Springer, Berlin/Heidelberg/New York.

Pfiffner, O.A., Ramsay, J.G., 1982. Constraints on geological strain rates—arguments from finite strain states of naturally deformed rocks. Journal of Geophysical Research 87 (B1), 311–321.

Sarantschina, G.M., 1963. Die Federow-Methode. VEB Deutscher Verlag der Wissenschaften, Berlin.

Sibson, R.H., 1975. Generation of pseudotachylite by ancient seismic faulting. Geophysical Journal of the Royal Astronomical Society 43, 775–794.

Spry, A., 1969. Metamorphic textures. Pergamon Press, Oxford.

Stipp, M., Stünitz, H., Heilbronner, R., Schmid, S.M., 2002a. The eastern Tonale fault zone: a 'natural laboratory' for crystal plastic deformation of quartz over a temperature range from 250 to 700°C. Journal of Structural Geology 24, 1861–1884.

Stipp, M., Stünitz, H., Heilbronner, R., Schmid, S.M., 2002b. Dynamic recrystallization of quartz: correlation between natural and experimental conditions. In: de Meer, S., Drury, M.R., de Bresser, J.H.P., Pennock, G.M. (Eds.), Deformation Mechanisms, Rheology and Tectonics: Current Status and Future Perspectives. Geological Society, London, Special Publications, vol. 200, pp. 171–190.

Stöckhert, B., Brix, M.R., Kleinschrodt, R., Hurford, A.J., Wirth, R., 1999. Thermochronometry and microstructures of quartz—a comparison with experimental flow laws and predictions on the temperature of the brittle-plastic transition. Journal of Structural Geology 21, 351–369.

Tribe, I.R., D'Lemos, R.S., 1996. Significance of a hiatus in down-temperature fabrics development within syntectonic quartz diorite complexes, Channel Islands, U.K. Journal of the Geological Society of London 153, 127–138.

Tullis, J., 1983. Deformation of feldspars. In: Ribbe, P.H. (Ed.), Feldspar Mineralogy, second ed.Reviews in Mineralogy 2 Mineralogical Society of America, pp. 297–323.

Tullis, J., Yund, R.A., 1987. Transition from cataclastic flow to dislocation creep of feldspar: mechanisms and microstructures. Geology 15, 606–609.

Urai, J.L., 1983. Deformation of wet salt rocks. Ph.D. thesis, University of Utrecht, The Netherlands.

Urai, J.L., Means, W.D., Lister, G.S., 1986. Dynamic recrystallization of minerals. In: Hobbs, B.E., Heard, H.C. (Eds.), Mineral and rock deformation: laboratory studies (The Paterson Volume). Geophysical Monograph 36. American Geophysical Union, pp. 161–199.

van Daalen, M., Heilbronner, R., Kunze, K., 1999. Orientation analysis of localized shear deformation in quartz fibres at the brittle-ductile transition. Tectonophysics 303, 83–107.

van Roermund, H.L.M., Konert, R.J., 1990. Deformation and recrystallization mechanisms in naturally deformed cordierite. Physics and Chemistry of Minerals 17, 52–61.

Vernon, R.H., 1991. Questions about myrmekite in deformed rocks. Journal of Structural Geology 13, 979–985.

Vernon, R.H., 2004. A practical guide to rock microstructure. Cambridge University Press, Cambridge/New York/Melbourne.

Vernon, R.H., Williams, V.A., D'Arcy, W.F., 1983. Grain size reduction and foliation development in a deformed granitoid batholith. Tectonophysics 92, 123–145.

Vernooij, M.G.C., Kunze, K., den Brok, B., 2006. 'Brittle' shear zones in experimentally deformed quartz single crystals. Journal of Structural Geology 28, 1292–1306.

Vielzeuf, D., 1983. The Spinel and quartz associations in high grade xenoliths from Tallanate (S.E. Spain) and their potential use in geothermometry and barometry. Contributions to Mineralogy and Petrology 82, 301–311.

Voll, G., 1960. New work on petrofabrics. Liverpool and Manchester Geological Journal 2, 503–567.

Voll, G., 1969. Klastische Mineralien aus den Sedimentserien der Schottischen Highlands und ihr Schicksal bei aufsteigender Regional- und Kontaktmetamorphose. Habilitationsschrift, Fakultät für Bergbau und Hüttenwesen, Technische Universität Berlin, D83.

Voll, G., 1976. Recrystallization of quartz, biotite and feldspars from Erstfeld to the Leventina Nappe, Swiss Alps, and its geological significance. Schweizerische mineralogische und petrographische Mitteilungen 56, 641–647.

von Federow, E., 1893. Nouvelle méthode pour l'étude goniométrique et optique des cristaux appliquée à la minéralogie et à la pétrographie. Mémoires du Comité Géologique X 2, 1–191.

Wirth, R., Voll, G., 1987. Cellular intergrowth between quartz and sodium-rich plagioclase (mymekite)—an analogue of discontinuous precipitation in metal alloys. Journal of Materials Science 22, 1913–1918.